

Analysis of orographic precipitation and isotopes in the vicinity of the South-Central Andes (latitude 37.6 to 32.4 S)

Mark T. Brandon¹, Lucas M. Fennell², and Michael T. Hren³

Corresponding author: Mark Brandon mark.brandon@yale.edu

¹ Department of Earth and Planetary Sciences, Yale University, New Haven CT 06520

² CONICET - Universidad de Buenos Aires. Instituto de Estudios Andinos Don Pablo Groeber (IDEAN). Intendente Güiraldes 2160, Pabellón II, 1428, Buenos Aires, Argentina

³ Michael T. Hren, Department of Geosciences, University of Connecticut, Storrs, CT 06269

Overview

The “altitude effect” (Dansgaard, 1964) describes the common observation that the stable isotope composition of hydrogen and oxygen in precipitation tends to have a strong linear correlation with elevation of the sample. An early example of this linear relation is from Ambach et al., (1968), who show a linear relation for the isotopic composition of precipitation and glacial ice as a function of elevation along modern glaciers in the Alps.

This empirical relationship has been widely used for almost three decades now to study the topographic evolution of mountain ranges over geologic time (e.g., Drummond et al., 1993; Norris et al., 1999; Garzione et al., 2000; Poage and Chamberlain, 2001; Rowley et al., 2001; Blisniuk and Stern, 2005; Rowley and Garizone, 2007). Norris et al. (1999) coined the term *isotope paleoaltimetry*. We prefer the term *isotope paleotopography*, because the isotopic fractionation occurs as moist air moves across the topography, and thus the amount of fractionation is only loosely linked to the elevation where the precipitation reaches the Earth’s surface.

Atmospheric science provides support for this idea in that winds are forced to rise as they pass over mountainous topography, and this lifting leads to an “orographic enhancement” in the precipitation rate (e.g., Smith and Barstad, 2004; Smith and Evans, 2007). Stable-isotope data provide a measure of this lifting given that the isotopic composition of water vapor in an air parcel and the precipitation that falls from that parcel become progressively lighter as the parcel moves downwind over progressively higher topography. The decrease in the $\delta^2\text{H}$ and $\delta^{18}\text{O}$ of precipitation is often considered to be linearly related to the local elevation where the precipitation reached the ground, and this observation is often described by an *isotopic lapse rate*, which represents the decrease in $\delta^2\text{H}$ and $\delta^{18}\text{O}$ isotopic ratio per kilometer of elevation. Poage and Chamberlain (2001) report a global compilation of stable isotopic data for meteoric water, and they suggest the global average isotopic lapse rate for $\delta^{18}\text{O}$ is 2.8 ‰/km. The 8:1 slope of the meteoric water indicates that the lapse rate for $\delta^2\text{H}$ should be about 22 ‰/km.

An implicit assumption of the isotope-paleotopography approach is that precipitation is created by stratified flow over the topography. Poulsen et al. (2010) argue that this assumption is not tenable in areas, such as the tropics, where a significant amount of precipitation is associated

with convective instabilities. The mid-latitudes are affected by baroclinic instabilities (Holton and Hakim, 2013), which give rise to the migrating weather fronts and synoptic-scale precipitation events that distinguish this region. Both instabilities are caused by dynamic interactions within the atmosphere, and thus are poorly correlated with the underlying topography. The wind field associated with these instabilities may carry them over mountainous topography, which would enhance or diminish the precipitation rate depending on whether the flow was upslope or downslope, respectively.

These observations lead to the following interpretation. If convective and baroclinic instabilities are uncorrelated with topography, then the time-averaged precipitation rate associated with these instabilities should tend towards an approximately uniform value at a regional scale. In turn, precipitation formed by orographic lifting should be strongly correlated with the underlying topography, so the spatial distribution of time-averaged precipitation rates should be approximately fixed relative to the underlying topography. If the distribution of orographically-induced precipitation is stationary, then spatial distribution of the precipitation isotopes should be stationary as well.

Another criticism of isotope-paleotopography comes from Galewsky (2008, 2009), who argues that the size of large mountain ranges results in partial blocking of the air flow over the topography, and this, in turn, reduces the amount of orographic lifting and the isotopic lapse rates as well. There is no doubt that topographic blocking is an important phenomenon. It was first recognized in the 1940s by glider pilots and by focused studies on mountain meteorology (see historical summaries in Smith, 2003, and Grubišić and Lewis, 2004). Thus, Galewsky's criticism is well founded. What is not yet resolved is if blocking has a significant influence on the long-term time-averaged spatial distribution of precipitation isotopes. Our analysis here provides some diagnostics, which we use to address this issue for our South-Central Andes study. Given the importance of this question, we continue with a description of the blocking phenomenon.

Topographic Blocking

Topographic blocking is often represented by a diagnostic variable, called the mountain-height number (Smith, 2003), which is defined by $M = N_m H_{\max} / U$, where U is the horizontal wind speed, H_{\max} is the maximum elevation in the study area, and N_m is the moist buoyancy frequency (the moist quantity is used here because precipitation requires saturated air; see Durran and Klemp, 1982). When M is small relative to one, the wind field tends to flow up and over the mountain topography. As M approaches one, the wind field will start to be deflected laterally around the mountain topography, which means that there is less lifting and less precipitation. As M exceeds about 1.2 to 1.5, the wind field transitions to a nonlinear regime, which is marked by unsteady vortices and eddies, and breaking waves above the leeside of the mountain.

M is defined at the scale of the full model domain. We find it more useful to use a local measure of blocking, defined by the horizontal wind speed ratio at a point. The concept is simple, but some background is needed before this ratio is defined. Let's consider a simplified definition of the problem, where an arbitrary mountain range lies within a much larger wind field. At the regional scale, the wind field is characterized by a uniform and steady horizontal wind velocity with a magnitude U . In the modeling discussed below, we call this the base-state wind field (see Brandon, 2022, for details). Next, we define a right-handed coordinate system with the x axis

oriented in the downwind horizontal direction of the base-state wind field. The y axis is horizontal and normal to the x axis, and the z axis is vertical and up. The wind vector at an x, y, z point is defined by velocity components u , v , and w (which are referenced to the x , y , and z axes, respectively). As an example, the base-state wind field is uniform across the model domain, so the velocity components are uniform as well, with $u = U$, and $v = w = 0$. If we insert the mountain topography into this wind field, the wind velocity field is perturbed to new values for $u(x,y,z)$, $v(x, y, z)$, $w(x, y, z)$. The practice is to focus on perturbed components of the wind field, which are given by $u' = u - U$, $v' = v$, and $w' = w$. (See Holton and Hakim, 2013, chap. 5 for an excellent summary of the use of perturbation variables for modeling atmospheric flow.)

For analysis of topographic blocking, we focus on how u varies relative to U . With this in mind, we define the horizontal velocity ratio as u'/U . If we use the term in a strict sense, then blocking would describe locations where $u'/U \leq -1$, which means that horizontal wind speed parallel to the base-state wind direction is stalled at zero ($u = 0$) or has a reverse sense of flow ($u < 0$) relative to the base-state.

Blocking is usually associated with slow or reversed low-level winds over the windward side of a mountain and fast low-level winds over the leeward side. Thus, as a diagnostic, we can be confident that block is insignificant if the horizontal velocity ratio lies in the range $-1 < u'/U < 1$.

In the analysis below, we construct a map that shows the distribution of u'/U at the land surface. The reason is that magnitude of this ratio decreases upward from a point on the land surface, so the view at the bottom of the atmosphere is sufficient to determine where blocking might be a problem.

This study

The analysis reported here is designed to support an investigation of the Cenozoic evolution of topography in Argentina at the latitude of 35.5 S (Fennell et al., 2022). The Fennell et al. study is based on a detailed stratigraphic record (55 to 10 Ma) of the hydrogen isotopic composition, $\delta^2\text{H}$, of ancient precipitation, as recorded in samples of hydrated volcanic glass collected near Malargüe, Argentina. The hydration of volcanic glass is estimated to occur over a time scale of 1 to 10 ka, so our analysis should be focused on estimating the time-averaged spatial distribution of precipitation isotopes.

Our analysis is based on a compilation of isotopic analyses of modern meteoric water from a 365 x 575 km area surrounding Malargüe. These data are made available here in an Excel spreadsheet, entitled “Mendoza area water isotopes (32-38S) 10 Sep 2019.xlsx”.

The compilation contains isotope analyses for 589 unique locations, of which 83 are new, and 506 are from the published literature (references for the published data are given in the section below, entitled “References for Water Isotope Data”). Our compilation is focused on samples that are representative of the long-term average of precipitation isotopes in the vicinity of the sample location. We distinguish between “local” samples, where precipitation was collected at a single point, and “catchment” samples, where water samples were collected from rivers.

There are 49 local samples of precipitation. The reported isotopic compositions for these samples are averages for a sequence of monthly analyses. The averages were weighted by monthly precipitation when that information was available.

Most of the remaining samples are from rivers, and thus are catchment samples. For these, we have tried to focus on samples that were collected during base flow (summer months), because base flow in rivers is sourced by discharge of ground water from the subsurface. Natural ground water originates from precipitation that falls within the upslope catchment above the sample location. The residence time of ground water that discharges in small catchments is estimated to be about 1 to 3 years (McGuire and others, 2005), which indicates that the water and its stable isotopes are averaged over many precipitation events.

These data were reduced to a subset of analyses for 197 unique locations. The selection process is described below. Note that the Excel spreadsheet contains details about the decision to select or reject.

Selection Criteria

- 1) Our study requires paired measurements of $\delta^2\text{H}$ and $\delta^{18}\text{O}$ for each sample. Samples that lacked one of these measurements were rejected.
- 2) The original data generally include information about the elevation of each sample. We assessed the reliability of the reported locations by comparing the reported elevation, with an elevation calculated from a high-resolution digital elevation model using the reported longitude and latitude. A sample was rejected when there was a significant difference between these two elevations, and if it was not possible to correct the location.
- 3) Samples of glacial ice or direct runoff from a glacier, and samples that were collected near agricultural settings, ponds, or lakes were rejected.
- 4) Samples with isotopic compositions that are anomalously low or high relative to other nearby samples were rejected.
- 5) Samples based on time series of precipitation isotopes that are shorter than 20 months were rejected. As a result, of the 49 local samples indicated above, only 3 were from long enough records to be accepted.
- 6) In cases where samples were collected near a confluence in a river, we rejected the trunk sample, and used the tributary sample. In addition, the location for the tributary sample was shifted slightly upstream (no more than 1000 m) to ensure that the catchment calculation can isolate the upstream catchment of the tributary alone. The tributary samples are preferred given that they represent more localized samples of the precipitation field.
- 7) Individual analysis with “deuterium excess”, d_{excess} , less than 5 per mil were rejected. This cutoff is often used to distinguish between primary samples ($d_{\text{excess}} > 5$ per mil), which are defined as samples with isotopic compositions formed by condensation and

precipitation alone, and samples altered by subsequent evaporation ($d_{\text{excess}} < 5$ per mil). Chang et al. (2022) provides evidence from a large set of meteoric water samples that this threshold provides a reliable separation between primary and altered samples.

- 8) Replicate analyses were averaged to get a single value for each location. One might consider using these replicates to estimate errors and develop statistical weights for each sample location. We did not do this because we have found, from our least-squares estimates, that the uncertainties associated with the determination of the stable isotope concentrations are much smaller than the total error associate with each sample. The reason is that the total error is dominated by natural variation.

Results of OPI Analysis

We used the Orographic Precipitation and Isotope (OPI) programs of Brandon (2022) to analyze the 197 primary samples from our Malargüe study area. The OPI programs provides full representation of the steady flow of moist air over an arbitrary 3D topography, and the down-wind evolution of cloud water, precipitation, and stable isotope concentrations associated with that flow. The catchment region is calculated for each catchment sample, and used to integrate the precipitation and precipitation isotopes captured by the catchment.

The OPI programs include the capability to find a least-squares fit of the meteoric water isotope data relative to the model, and a best-fit estimate of a set of OPI parameters. A “one-wind” solution is defined by nine parameters: mean wind speed U , mean wind direction *azimuth*, sea-level surface-air temperature T_0 , mountain-height number M , horizontal eddy diffusivity κ , mean residence time for cloud water τ_c , the hydrogen isotopic composition of base precipitation at the centroid of the sample data $\delta^2\text{H}_0$, the latitudinal gradient of hydrogen isotopic composition of base precipitation $d(\delta^2\text{H}) / d(\text{latitude})$, and the fraction of precipitation remaining after evaporation f_p .

Our study here uses a “two-wind” solution, which is defined by a set of nineteen parameters. This set is simply a mixture of two “one-wind” solutions (9 parameters \times 2) plus an addition parameter that describes the proportion of the total precipitation field that is associated with the first “one-wind” solution.

The output from OPI programs is reported in full below. Those readers interested in the details are encouraged to read the description provided in Brandon (2022) for the design of the OPI programs, the definition of terminology and parameters, and the interpretation of results.

We follow with a summary of the main conclusions, with an emphasis on those points that are most relevant for the Fennell et al. (2022) paper.

- 1) We conducted about 55 runs to test and confirm the best-fit OPI solution for the South-Central Andes isotope data. Early runs were focused on testing and debugging the OPI “two-winds” calculation. The middle set of runs were focused on developing a sensible algorithm and parameterization for representing evaporative recycling during precipitation events. The last set of runs were focused on evaluating “one-wind” and “two-wind” solutions, and ensuring the direct-search algorithm for the least-squares fit

had found a unique, well-defined “two-wind” solution. Note that a two-winds least-squares solution takes about 8 days on a cluster with 27 CPUs running in parallel, so this testing is important but also fairly time consuming.

- 2) The runs clearly indicate that the isotope data are best-fit by a “two-winds” solution. The best-fit solution indicates that the errors for the stable isotope data have standard deviations of 11.2 per mil for $\delta^2\text{H}$ and 1.3 per mil for $\delta^{18}\text{O}$. The figures produced by opiPlots_TwoWinds provides a good demonstration of the fit of the data relative to the model. The estimated parameters seem physically plausible and reasonable. Most parameters are well resolved (see uncertainties in the log page for opiPairPlots), except for the horizontal eddy diffusivity κ , and the average residence time for cloud water τ_c . Note that poor resolution of parameters would be a concern if we were comparing to direct measurements, but this is not a problem when making predictions. The reason is that that the poor resolution of a parameter indicates that predictions will be insensitive to the value of that parameter.

Precipitation State #1 (“Westerly Winds”)

Wind speed (m/s): 2.0 m/s

Azimuth: 91.4 degrees

Sea-level temperature: 291.2 K (18.1 °C)

Mountain-height number: 0.053 (dimensionless)

Horizontal eddy diffusivity: 17 m²/s

Average residence time for cloud water: 0 s

$\delta^2\text{H}$ for base precipitation: -15.1 per mil

$\delta^2\text{H}$ latitude gradient for base precipitation: -3.601 per mil/deg lat

Residual precipitation after evaporation: 1.00 (fraction)

Fraction for precipitation state #1: 0.29

Precipitation State #2 (“Northeasterly Winds”)

Wind speed (m/s): 3.0 m/s

Azimuth: 233.2 degrees

Sea-level temperature: 289.6 K (16.5 °C)

Mountain-height number: 0.265 (dimensionless)

Horizontal eddy diffusivity: 72558 m²/s

Average residence time for cloud water: 251 s

$\delta^2\text{H}$ for base precipitation: -7.9 per mil

$\delta^2\text{H}$ latitude gradient for base precipitation: -4.504 per mil/deg lat

Residual precipitation after evaporation: 0.98 (fraction)

- 3) The two-winds solution reported above includes estimates for evaporative recycling. The issue here is not about the primary samples, which were screened to avoid post-precipitation evaporation. Rather, these estimates indicate how much of the total precipitation that falls within the model domain is recycled back into the atmosphere. Much of this recycling occurs as precipitation falls through dry regions in the atmosphere. The efficiency of the precipitation process is reduced as the amount of evaporative recycling increases. Likewise, the amount of isotope fractionation is reduced as well. The best-fit solution indicates that

there was almost no evaporative loss associated with the two precipitation states. The relevant parameter is called “Residual precipitation after evaporation”, and the reported values for the westerly and northeasterly solutions are 1.0 and 0.98, respectively. These values indicate the fraction of precipitation that exits through the base of the model (as ground water). The complementary values, 0 and 0.02, indicate the fraction of the total precipitation that was recycled back into the atmosphere as water vapor. Interested readers are directed to Chang et al. (2022), which reports on a detailed study of evaporative recycling in the Patagonian Andes.

- 4) The OPI programs assume that all precipitation is due to stratiform flow of moist air over topography. The good fit of the model to the data suggests that this simplification is reasonable. But note that stratiform flow is expected given that our study area is in the subtropics.
- 5) The best-fit solution shows the mountain-height number, M , is 0.05 and 0.26 for the westerly and northeasterly sources, respectively. Figures 18 and 19 in *opiMaps_TwoWinds* present maps that show the horizontal velocity ratio, u'/U at the land surface. The magnitude $|u'/U|$ is less than 0.6. Likewise, the streamlines for the two wind fields (figures 3 and 4 in *opiMaps_TwoWinds*) pass undeflected over the mountain range. This evidence clearly indicates that topographic blocking is not a factor for the mean precipitation field over this part of the South-Central Andes. Our estimates for the moist buoyant frequency are $N_m = 0.016$ and 0.127 mrad/s for the westerly and northeasterly sources, respectively. Most authors envision a much larger average value for the buoyance frequency of the troposphere, equal to about 10 mrad/s (e.g., Holton and Hakim, 2013, p. 56). This result may resolve the debate of the influence of blocking on orographic precipitation in that the actual value for N_m is smaller than expected.
- 6) Figure 9 in *opiMaps_TwoWinds* shows that westerly moist air is able to cross the South-Central Andes. However, the OPI solution clearly shows that this westerly source does not produce precipitation when it flows down the east flank of the range. The reason is that downslope flow in this area causes the air to become strongly undersaturated. This conclusion is important because it indicates that precipitation in the Malargüe area is due to the northeasterly source, which causes upslope flow of moist air over the east flank of the range. Another interesting feature of this figure is that it shows that the westerly source creates precipitation where it flows up the western slopes of the basement highs of the Sierras Pampeanas.
- 7) Figure 5 shows a linear relationship between isotopic fractionation and local elevation, which is consistent with the concept of “isotope paleoaltimetry”. Figure 6 shows that there is a better fit when local elevation is replaced by *maximum lifting*, which is defined as the maximum elevation along the path upwind of the sample point. This result is especially important for the Fennell et al. study. The cross section along the northeasterly wind path (figure 6 from *opiMaps_TwoWinds*) passed through the Malargüe study area. The lower plot in figure 6 shows that much of the isotopic fractionation recorded by the precipitation occurs as moist wind flows over two of the basement highs in the Sierras Pampeanas (Sierras de San Luis and Córdoba) located upwind of Malargüe. The point to emphasize is that the isotopic

fractionation observed in Malargüe provides a record of the topography upwind of that location, rather than simply the elevation at Malargüe.

- 8) The best-fit OPI solution indicates an $\delta^2\text{H}$ isotopic lapse rate of 27 per mil/km for moisture reaching Malargüe (see log file for `opiPlots_TwoWinds`). This result is similar to the global estimate by Poage and Chamberlain (2001), which indicates a $\delta^2\text{H}$ lapse rate of 22 per mil/km.

Prediction of Precipitation Isotopes for Past Climate

The `opiPredict` program provides an estimate of how variations in climate would influence the isotopic composition of orographic precipitation. We have found that sea-level surface-air temperature, T_0 , has the strongest effect, and other climate variables, such as wind speed, wind direction, and buoyant stability, have little influence. This temperature sensitivity affects isotopic composition in two ways. The first is associated with base precipitation, which is defined as the precipitation that would occur if there were no topography (Brandon, 2022). The isotopic composition of this component of the precipitation will be heavier as temperature increases (e.g., figure 3 in Dansgaard, 1964). The second is the isotopic lapse rate. The OPI model shows that this rate decreases with increasing T_0 . Here we lay out a method that corrects for these two temperature sensitivities, and also provides an estimate of the average T_0 in a study area as a function latitude and age.

We propose the following scaling approximation for estimating the isotopic composition of base precipitation at a specified location sometime in the past,

$$\delta_{0,\text{past}} = \delta_{0,\text{present}} + s_{\text{base}}(T_{0,\text{past}} - T_{0,\text{present}}) + (\delta_{\text{sw},\text{past}} - \delta_{\text{sw},\text{present}})$$

where $\delta_{0,\text{present}}$ is the isotopic composition of the present base precipitation (known from the OPI solution), $T_{0,\text{present}}$ and $T_{0,\text{past}}$ are the present and past sea-level surface air temperature, and $\delta_{\text{sw},\text{present}}$ and $\delta_{\text{sw},\text{past}}$ are the present and past isotopic composition of seawater. The isotopic variables are shown in a generic fashion to indicate that the equation is applicable for both hydrogen and oxygen isotopes. The first term on the right side of the equation accounts for the effect of temperature on isotopic fractionation, and the second term on the right accounts for the change with age in the isotopic composition of the oceans. The evolution of δ_{sw} with age is provided by the benthic foraminifera record (e.g., Miller et al., 2020).

The coefficient s_{base} is estimated using the slope of the best-fit line for monthly measurements of $\delta^2\text{H}$ and $\delta^{18}\text{O}$ as a function of the monthly temperature. The justification for this estimate is that modern variations in the stable isotope composition of precipitation provides a useful estimate of the temperature sensitivity of this process (c.f., figure 3 in Dansgaard, 1964).

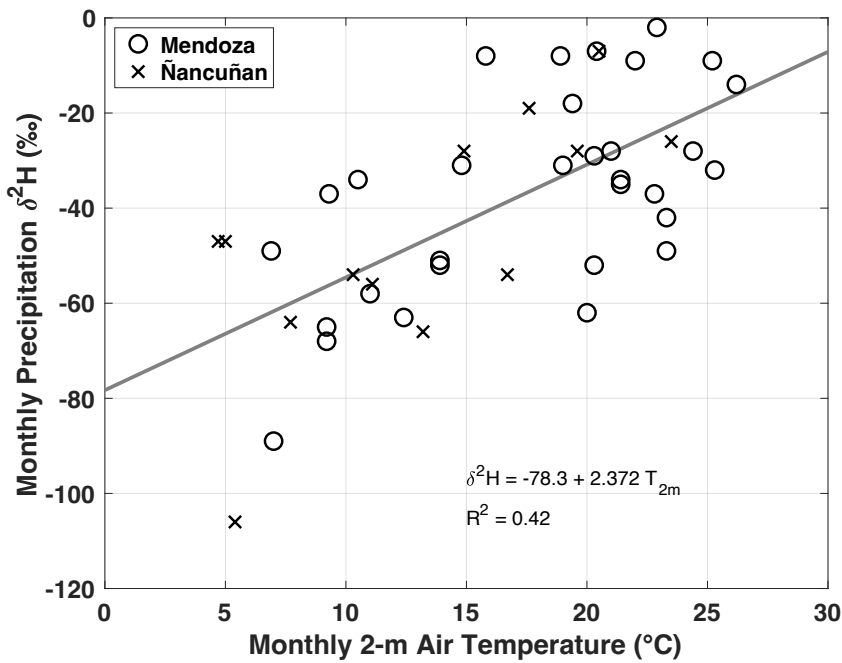


Figure 1. Monthly precipitation $\delta^2\text{H}$ versus Monthly surface-air temperature for GNIP stations at Mendoza and Ñancuñan, in western Argentina.

The Fennell et al. (2022) study is focused on the northeasterly wind solution, given that it is the source of moisture for the Malargüe site. The coefficient s_{base} is estimated using monthly data from the Mendoza and Ñancuñan GNIP stations, both of which are in the foreland east of the Main Cordillera. These data are shown above in figure 1. The slope of the best-fit line gives an estimate for $s_{base} = 2.37$ per mil/ $^{\circ}\text{C}$.

The OPI model is used to calculate the influence of T_0 on isotope fractionation associated with orographic precipitation. This is done by running the OPI model at 1 Ma increments over the duration of the Cenozoic. The parameters T_0 and $\delta^2\text{H}_0$ are varied as a function of age, but the topography and the other OPI parameters are maintained at their modern values.

The results of these calculations are shown in figure 1 from opiPredict. The gray curves in the top of the upper plot show the estimated evolution of $\delta^2\text{H}_0$ at the latitude of Malargüe with time. The blue curve represents a smoothed version of that evolution. The red points in the lower part of that plot show precipitation $\delta^2\text{H}$ values with age, as determined by the hydrated glass samples in Fennell et al. (2022). The blue line with points shows the precipitation $\delta^2\text{H}$ values from opiPredict. They represent the $\delta^2\text{H}$ values that would be observed if the topography remains the same as present. Thus, this lower blue should be viewed as a reference condition for interpretation of the observed data, shown as the red points. The observed $\delta^2\text{H}$ values that plot above the reference line would indicate less fractionation and lower topography, and those that plot below the reference line would indicate more fractionation and higher topography.

The lower plot in figure 1 from opiPredict shows the estimated T_0 record for Malargüe. This record was calculated using the Cenozoic temperature record from benthic foraminifera from Miller et al. (2020) and converting that record to the latitude of Malargüe using a moist energy balance model (MEBM) (Flannery, 1984; Roe et al., 2015; MATLAB code for MEBM provided by Gerard Roe, 2019). The MEBM we are using provides a zonally averaged estimate of the latitudinal variation of annual mean temperature as a function of radiative fluxes and a latitudinal heat flux driven by eddy diffusion. The isotopic composition of benthic foraminifera provides a record of temperate of the deep ocean (Miller et al., 2020). This “deep water is formed by the sinking of saline cold sea water from the surface of the global oceans at high latitudes. In the modern southern oceans, this convective downwelling occurs at about 56° latitude, which is the southern latitude where the zonally averaged sea-surface temperature is equal to the modern deep-water temperature (3.1°C , Miller et al., 2020).

We assume that, in the past, deep water was formed in the same fashion and at roughly the same latitude. If correct, then the benthic-foraminifera temperature record can be considered a record of the zonally averaged sea-surface temperature at about 56° latitude. To implement this idea, we solved for the variation in the outgoing long-wave radiation (OLR) in the MEBM to match the benthic foraminifera temperature record at 56° . The result of this calculation is reported in file “MEBM_vary_OLR.mat” in Brandon (2022), which contains latitudinal temperature profiles as a function of varying OLR. The file “Miller2020BenthicForamClimate.mat” contains the deep-water temperature and isotopic composition of seawater for the Cenozoic, as analyzed by Miller et al. (2020). opiPredict combines this information to generate the variation of T_0 with age at a specified latitude.

The gray curve in the lower plot from opiPredict shows T_0 as predicted for Malargüe at latitude 35.5° S. The blue curve shows a smoothed version of that curve. Note that we use the smoothed curves for our final calculations given that the ages of samples in Fennell et al. (2022) are not precise enough to match the age resolution of benthic-foraminifera record. opiPredict uses the difference between the high-resolution curve and the smooth curve to estimate the error caused for this difference in age resolution.

Figure 2 in opiPredict shows a simpler way to view the $\delta^2\text{H}$ record, provided by the hydrated glass samples from Malargüe. We introduce a new variable, the isotope fractionation ratio during lifting, defined by

$$\Phi_{\text{lift}} = \frac{\ln(1+\delta_{\text{past}}) - \ln(1+\delta_{0,\text{past}})}{\ln(1+\delta_{\text{past}}^*) - \ln(1+\delta_{0,\text{past}})} \approx \frac{\delta_{\text{past}} - \delta_{0,\text{past}}}{\delta_{\text{past}}^* - \delta_{0,\text{past}}}.$$

The central part of this equation gives the exact definition, and the part on the right shows the calculation using the usual delta approximation for logarithms. The variable δ_{past} is the isotopic composition measured for a sample from a specified location and age (e.g., the precipitation $\delta^2\text{H}$ recorded by hydrated glass). $\delta_{0,\text{past}}$ is the isotopic composition of the base precipitation at that same location and age. δ_{past}^* is the isotopic composition predicted by opiPredict for that location and age, but with the topography unchanged relative to present.

In other words, Φ_{lift} is the ratio of the observed isotopic fractionation due to orographic lifting at a specified location and age, relative to the predicted fractionation that would be observed at that

age if there were no change in topography. The OPI model shows that there is a linear relationship between isotopic fractionation and maximum lifting (e.g., figure 4 from `opiPlots_TwoWinds`). As a result, Φ_{lift} is a measure of the change in the past upwind topography relative to that for the modern. For example, the results from Fennell et al. (2022) indicate that $\Phi_{lift} \approx 0.5$ at about 10 Ma, which means that the topography along the upwind path (pointing to the northeast) was 50 % lower than the modern topography along that upwind path.

Acknowledgements

We thank Gerard Roe for sharing his MATLAB version of a moist-energy balance model for the modern Earth. The research was supported in part by Fulbright Fellowship to Lucas Fennell, and by US National Science Foundation grants, NSF EAR-1650313 and EAR-1650396 to Mark Brandon and Michael Hren, respectively.

General References

Ambach, W., W. Dansgaard, H. Eisner & J. Møller (1968) The altitude effect on the isotopic composition of precipitation and glacier ice in the Alps, *Tellus*, 20:4, 595–600, DOI: 10.3402/tellusa.v20i4.10040

Blisniuk, P., and Stern, L., 2005, Stable isotope paleoaltimetry: A critical review: *American Journal of Science*, v. 305, p. 1033.

Brandon, M.T., 2022, MATLAB Programs for the Analysis of Orographic Precipitation and Isotopes, with Implications for the Study of Paleotopography, doi: 10.5281/zenodo.7076557, <https://github.com/foret37/OPI-Orographic-Precipitation-and-Isotopes/tree/v3.6.002>.

Chamberlain, C.P. and Poage, M.A., 2000. Reconstructing the paleotopography of mountain belts from the isotopic composition of authigenic minerals. *Geology*, 28(2), pp.115-118.

Chang, Q., Brandon, M.T., and Hren, M.T., 2022, Topography, Evaporation and Precipitation Isotopes Across the Patagonian Andes (in review).

Durran, D., and Klemp, J., 1982, On the effects of moisture on the Brunt–Vaisala frequency: *Journal of the Atmospheric Sciences*, v. 39, p. 2152–2158.

Dansgaard, W., 1964, Stable isotopes in precipitation: *Tellus*, v. 16, p. 436–468.

Drummond, C. N., Wilkinson, B. H., Lohmann, K. C., and Smith, G. R., 1993, Effect of regional topography and hydrology on the lacustrine isotopic record of Miocene paleoclimate in the Rocky Mountains: *Palaeogeography, Palaeoclimatology, Palaeoecology*, v. 101, p. 67–79.

Durran, D., and Klemp, J., 1982, On the effects of moisture on the Brunt–Vaisala frequency: *Journal of the Atmospheric Sciences*, v. 39, p. 2152–2158.

Fennell, L.M., Brandon, M.T., and Hren, M.T., 2022, Cenozoic topographic evolution of the Southern Central Andes foreland region as revealed by hydrogen stable isotopes in hydrated volcanic glass (in review).

Flannery, B. P., 1984, Energy balance models incorporating transport of thermal and latent energy: *Journal of the Atmospheric Sciences*, v. 41, p. 414–421.

Garzione, C. N., Dettman, D. L., Quade, J., DeCelles, P. G., and Butler, R. F., 2000, High times on the Tibetan Plateau: Paleoelevation of the Thakkhola graben, Nepal: *Geology*, v. 28, p. 339–342.

Holton, J. R., and Hakim, G. J., 2013, *An Introduction to Dynamic Meteorology*: Academic Press, Academic Press.

McGuire, K. J., McDonnell, J. J., Weiler, M., Kendall, C., McGlynn, B. L., Welker, J. M., and Seibert, J., 2005, The role of topography on catchment scale water residence time: *Water Resources Research*, v. 41, no. 5, DOI:10.1029/2004WR003657.

Miller, K. G., Browning, J. V., Schmelz, W. J., Kopp, R. E., Mountain, G. S., and Wright, J. D., 2020, Cenozoic sea-level and cryospheric evolution from deep-sea geochemical and continental margin records: *Science Advances*, v. 6, p. eaaz1346.

Norris, R. D., Corfield, R. M., and Hayes-Baker, K., 1999, Mountains and Eocene climate, *in*, p. 161–196.

Roe, G. H., Feldl, N., Armour, K. C., Hwang, Y.-T., and Frierson, D. M. W., 2015, The remote impacts of climate feedbacks on regional climate predictability: *Nature Publishing Group*, v. 8, p. 135–139.

Rowley, D., Pierrehumbert, R., and Currie, B., 2001, A new approach to stable isotope-based paleoaltimetry: implications for paleoaltimetry and paleohypsometry of the High Himalaya since the Late Miocene: *Earth and Planetary Science Letters*, v. 188, p. 253–268.

Rowley, D. B., and Garzione, C. N., 2007, Stable isotope-based paleoaltimetry: *Annual Review of Earth and Planetary Sciences*, v. 35, p. 463–508.

Poage, M., and Chamberlain, C., 2001, Empirical relationships between elevation and the stable isotope composition of precipitation and surface waters: Considerations for studies of paleoelevation change: *American Journal of Science*, v. 301, p. 1–15.

Poulsen, C. J., Ehlers, T. A., and Insel, N., 2010, Onset of Convective Rainfall During Gradual Late Miocene Rise of the Central Andes: *Science*, v. 328, p. 490.

Smith, R. B., 2003, Stratified flow over topography, *in* Environmental stratified flows: Springer, Boston, MA, p. 119–159.

Smith, R. B., and Barstad, I., 2004, A Linear Theory of Orographic Precipitation: *Journal of the Atmospheric Sciences*, v. 61, p. 1377–1391.

Smith, R. B., and Evans, J., 2007, Orographic precipitation and water vapor fractionation over the southern Andes: *Journal of Hydrometeorology*, v. 8, p. 3–19.

References for Water Isotope Data

- Crespo, S., Aranibar, J., Gomez, L., Schwikowski, M., Bruetsch, S., Cara, L., Villalba, R., 2017. Ionic and stable isotope chemistry as indicators of water sources to the Upper Mendoza River basin, Central Andes of Argentina. *Hydrological Sciences Journal* 62, 588–605.
<https://doi.org/10.1080/02626667.2016.1252840>
- Fernández, E., Grilli, A., Alvarez, D., Aravena, R., 2017. Evaluation of nitrate levels in groundwater under agricultural fields in two pilot areas in central Chile: A hydrogeological and geochemical approach. *Hydrological Processes* 31, 1206–1224.
<https://doi.org/10.1002/hyp.11103>
- Hoke, G.D., Aranibar, J.N., Viale, M., Araneo, D.C., Llano, C., 2013. Seasonal moisture sources and the isotopic composition of precipitation, rivers, and carbonates across the Andes at 32.5–35.5°S. *Geochemistry, Geophysics, Geosystems* 14, 962–978.
<https://doi.org/10.1002/ggge.20045>
- Markovich, K.H., Dahlke, H.E., Arumí, J.L., Maxwell, R.M., Fogg, G.E., 2019. Bayesian hydrograph separation in a minimally gauged alpine volcanic watershed in central Chile. *Journal of Hydrology* 575, 1288–1300. <https://doi.org/10.1016/j.jhydrol.2019.06.014>
- Ohlanders, N., Rodriguez, M., McPhee, J., 2013. Stable water isotope variation in a Central Andean watershed dominated by glacier and snowmelt. *Hydrology and Earth System Sciences* 17, 1035–1050. <https://doi.org/10.5194/hess-17-1035-2013>
- Ostera, H.A., Dapeña, C., 2003. Environmental Isotopes and Geochemistry of Bañado Carilauquen, Mendoza, Argentina, in: IV South American Symposium on Isotope Geology. pp. 461–464.
- Panarello, H.O., Dapeña, C., 1996. Mecanismos de recarga y salinización en las cuencas del Río Mendoza y Tunuyán, Mendoza, República Argentina: evidenciados por isótopos ambientales, in: XII Congreso Geológico de Bolivia. pp. 531–543.
- Sánchez-Murillo, R., Aguirre-Dueñas, E., Gallardo-Amestica, M., Moya-Vega, P., Birkel, C., Esquivel-Hernández, G., Boll, J., 2018. Isotopic characterization of Waters across Chile, in: Rivera, D.A., Godoy-Faundez, A., Lillo-Saavedra, M. (Eds.), *Andean Hydrology*. pp. 205–230. <https://doi.org/10.1201/9781315155982>
- Sanci, R., Panarello, H.O., Ostera, H.A., 2010. Flujo de dióxido de carbono en el flanco oriental del volcán peteroa, andes del sur. *Revista Mexicana de Ciencias Geológicas* 27, 225–237.
- Sileo, N., Trombotto, D., Dapeña, C., 2015. Estudios preliminares del agua, nieve y hielo en la cuenca del río Vallecitos, Mendoza, Argentina. *Acta geológica lilloana* 27, 130–145.

Ugan, A., Neme, G., Gil, A., Coltrain, J., Tykot, R., Novellino, P., 2012. Geographic variation in bone carbonate and water $\delta^{18}\text{O}$ values in Mendoza, Argentina and their relationship to prehistoric economy and settlement. *Journal of Archaeological Science* 39, 2752–2763.
<https://doi.org/10.1016/j.jas.2012.04.013>

Program: opiFit_TwoWinds
Start time: 24-Jul-2022 23:58:28
Run file path:
run043_Mendoza
Run filename:
run043.run
Run title:
run 043, Mendoza area, opi 3.6, two wind, leeside evaporation, fit for kappa
Path name for data directory:
~/project/OPI/data Mendoza

opiFit_TwoWinds

----- Topography File -----
Topography file: Mendoza topography_Gebco1km_-85,-43,-42.5,-27.5.mat
Maximum elevation (m): 6317.73
Grid size, nx and ny: 3827, 1669
Minimum and maximum for longitude: -85, -43
Minimum and maximum for latitude: -42.5, -27.5
Grid spacing, dx and dy (degrees): 0.0109775, 0.00899281
Grid spacing, dx and dy (km): 0.999894, 0.999954
Size of cosine window as fraction of grid size: 0.250000
Lon, lat for map origin (degrees): -70.2402, -34.3854
Map origin is set to sample centroid.
Coriolis frequency at map-center latitude (mrad/s): -0.0823652
Lon, lat for section origin (degrees): -69.61, -35.14

----- Sample File -----
Sample file: Mendoza area water isotopes (32-38S) 10 Sep 2019.xlsx
Number of all samples: 197
Number of altered samples: 0
Number of primary samples: 197
Number of local primary samples: 3
Number of catchment primary samples: 194
Minimum and maximum for longitude: -72.092, -68.07
Minimum and maximum for latitude: -37.5851, -32.3746

----- Constants -----
Characteristic distance for isotopic exchange (m): 540
Standard-deviation ratio for data residuals: 28.3

----- Constraints for Best-Fit Solution -----
Precipitation State 1:
Wind speed (m/s): 0.1, 20
Wind azimuth (degrees): 35, 145
Sea-level temperature (K): 270, 300
Mountain-Height Number (dimensionless): 0, 1.2
Horizontal eddy diffusivity (m^2/s): 0, 1e+06
Characteristic condensation time (s): 0, 2500
d2H for base precipitation (per mil): -60, 0
d2H latitude gradient for base precipitation (per mil/deg lat): -15, 0
Residual precipitation after evaporation (fraction): 0, 1
Fraction for precipitation state #1: 0, 1

Precipitation State 2:
Wind speed (m/s): 0.1, 20
Wind azimuth (degrees): 215, 325

Sea-level temperature (K): 270, 300
Mountain-Height Number (dimensionless): 0, 1.2
Horizontal eddy diffusivity (m^2/s): 0, 1e+06
Characteristic condensation time (s): 0, 2500
 $d2H$ for base precipitation (per mil): -60, 0
 $d2H$ latitude gradient for base precipitation (per mil/deg lat): -15, 0
Residual precipitation after evaporation (fraction): 0, 1

----- Evaporation Option -----

Leeside evaporative recycling for both precipitation states.

----- Solutions From Restart File -----

Restart file: 07_opiFit_Solutions.txt
Title for solutions in restart file:
run 043, Mendoza area, opi 3.6, two wind, leeside evaporation, fit for kappa
Number of restart solutions: 115081

----- Best-Fit Search -----

Starting parallel pool (parpool) using the 'local' profile ...
Connected to the parallel pool (number of workers: 27).
Modified controlled random search, fminCRSS3
Number of parameters = 19
Number of free parameters = 19
Factor for size of search set, mu = 10
Size of search set = 200
Specified epsilon for stopping criterion = 0.0001
Workers for parallel calculation = 27

Parallel pool using the 'local' profile is shutting down.

----- Estimates for Best-Fit Solution -----

Precipitation State 1:
Wind speed (m/s): 1.95495
Azimuth (degrees): 91.3531
Sea-level temperature (K): 291.215
Mountain-height number (dimensionless): 0.052755
Horizontal eddy diffusivity (m^2/s): 17.0072
Average residence time for cloud water (s): 0.0158616
 $d2H$ for base precipitation (per mil): -15.1117
 $d2H$ latitude gradient for base precipitation (per mil/deg lat): -3.60092
Residual precipitation after evaporation (fraction): 0.999903
Fraction for precipitation state #1: 0.289365

Precipitation State 2:

Wind speed (m/s): 3.0204
Azimuth (degrees): 233.228
Sea-level temperature (K): 289.614
Mountain-height number (dimensionless): 0.265313
Horizontal eddy diffusivity (m^2/s): 72557.6
Average residence time for cloud water (s): 250.814
 $d2H$ for base precipitation (per mil): -7.88753
 $d2H$ latitude gradient for base precipitation (per mil/deg lat): -4.50388
Residual precipitation after evaporation (fraction): 0.975209

---- Other Variables Related to Best-Fit Solution ---

Precipitation State 1:

Saturated buoyancy frequency (rad/s): 1.63244e-05
d180 for base precipitation (per mil): -3.22076
d180 latitude gradient for base precipitation (per mil/deg lat): -0.442557
Average residence time for falling precipitation (s): 1408.82
Water-vapor density at sea level (g/m^3): 15.6159
Scale height for water vapor (m): 3008.4
Average velocity for falling precipitation (m/s): 2.1354
Total density at sea level (g/m^3): 1.2111
Scale height for total density (m): 9733.610703
Average lapse-rate ratio, gammaSat/gammaEnv: 0.915021

Precipitation State 2:

Saturated buoyancy frequency (rad/s): 0.000126842
d180 for base precipitation (per mil): -2.3329
d180 latitude gradient for base precipitation (per mil/deg lat): -0.553531
Average residence time for falling precipitation (s): 1346.49
Water-vapor density at sea level (g/m^3): 14.1888
Scale height for water vapor (m): 2883.25
Average velocity for falling precipitation (m/s): 2.14131
Total density at sea level (g/m^3): 1.21927
Scale height for total density (m): 9705.307145
Average lapse-rate ratio, gammaSat/gammaEnv: 0.920506

----- Observed Meteoric Water Line -----

Principal standard deviations (per mil): 0.338403, 31.213
Intercept and slope (per mil): 11.0944, 8.13663

----- Predicted Meteoric Water Line -----

Principal standard deviations (per mil): 0.175692, 27.8014
Intercept and slope (per mil): 10.9427, 8.10226

----- Quality of Fit -----

Reduced chi-square: 2.33505

Degrees of freedom: 178

Number for primary samples in wet locations: 197

Number of primary samples: 197

Best-fit parameters:

1.95495 91.3531 291.215 0.052755 17.0072 0.0158616 -0.0151117 -0.00360092 0.999903
0.289365 3.0204 233.228 289.614 0.265313 72557.6 250.814 -0.00788753 -0.00450388
0.975209

Finish time: 25-Jul-2022 05:03:55

Program: opiCalc_TwoWinds
Start time: 07-Sep-2022 23:26:58

Run file path:

/Users/markbrandon/Dropbox (Yale University)/OPI Mendoza/runs/run043_Mendoza, leeside evaporation, fit for kappa BEST SOLUTION

Run file name:

run043.run

Run title:

run 043, Mendoza area, opi 3.6, two wind, leeside evaporation, fit for kappa

Path name for data directory:

~/Dropbox/OPI Mendoza/data Mendoza

opiCalc_TwoWinds

----- Topography File -----

Topography file: Mendoza topography_Gebco1km_-85,-43,-42.5,-27.5.mat

Maximum elevation: 6318 m

Grid size, nx and ny: 3827, 1669

Minimum and maximum for longitude: -85.00000, -43.00000 degrees

Minimum and maximum for latitude: -42.50000, -27.50000 degrees

Grid spacing, dLon and dLat: 0.01098, 0.00899 degrees

Grid spacing, dx and dy: 1.01, 1.00 km

Lon, lat for map origin: -70.24021, -34.38537 degrees

Map origin is set to sample centroid.

Size of cosine window as fraction of grid size: 0.25 (dimensionless)

Coriolis frequency at map-origin latitude (mrad/s): -0.082

Lon, lat for section origin (degrees): -69.61000, -35.14000

----- Sample File -----

Sample file: Mendoza area water isotopes (32-38S) 10 Sep 2019.xlsx

Number of all samples: 197

Number of primary samples: 197

Number of local primary samples: 3

Number of catchment primary samples: 194

Number of altered samples: 0

Centroid for primary samples, longitude, latitude: -70.24021, -34.38537 degrees

Minimum and maximum for longitude: -72.09199, -68.07000

Minimum and maximum for latitude: -37.58512, -32.37459

----- Constants -----

Characteristic distance for isotopic exchange: 540 m

Standard-deviation ratio for data residuals: 28.30 (dimensionless)

----- Constraints for Best-Fit Solution -----

Precipitation State #1:

Wind speed: 0.1, 20 m/s

Wind azimuth: 35, 145 degrees

Sea-level surface-air temperature: 270, 300 K (-3.1, 26.9 °C)

Mountain-height number: 0, 1.2 (dimensionless)

Horizontal eddy diffusivity: 0, 1e+06 m^2/s

Average condensation time (s): 0, 2500 s

d2H for base precipitation: -60, 0 per mil

d2H latitude gradient for base precipitation: -15, 0 per mil/deg lat

Residual precipitation after evaporation: 0, 1 (fraction)

Fraction for precipitation state 1: 0, 1

Precipitation State #2:

Wind speed: 0.1, 20 m/s
Wind azimuth: 215, 325 degrees
Sea-level surface-air temperature: 270, 300 K (-3.1, 26.9 °C)
Mountain-height number (dimensionless): 0, 1.2
Horizontal eddy diffusivity: 0, 1e+06 m^2/s
Average condensation time: 0, 2500 s
d2H for base precipitation: -60, 0 per mil
d2H latitude gradient for base precipitation: -15, 0 per mil/deg lat
Residual precipitation after evaporation: 0, 1 (fraction)

----- Evaporation Option -----
Evaporative recycling active for both precipitation states.

----- Solution -----
Precipitation State #1:
Wind speed (m/s): 2.0 m/s
Azimuth: 91.4 degrees
Sea-level temperature: 291.2 K (18.1 °C)
Mountain-height number: 0.053 (dimensionless)
Horizontal eddy diffusivity: 17 m^2/s
Average residence time for cloud water: 0 s
d2H for base precipitation: -15.1 per mil
d2H latitude gradient for base precipitation: -3.601 per mil/deg lat
Residual precipitation after evaporation: 1.00 (fraction)
Fraction for precipitation state #1: 0.29

Precipitation State #2:
Wind speed (m/s): 3.0 m/s
Azimuth: 233.2 degrees
Sea-level temperature: 289.6 K (16.5 °C)
Mountain-height number: 0.265 (dimensionless)
Horizontal eddy diffusivity: 72558 m^2/s
Average residence time for cloud water: 251 s
d2H for base precipitation: -7.9 per mil
d2H latitude gradient for base precipitation: -4.504 per mil/deg lat
Residual precipitation after evaporation: 0.98 (fraction)

---- Other Variables Related to Best-Fit Solution ---
Precipitation State #1:
Moist buoyancy frequency: 0.016 mrad/s
d180 for base precipitation: -3.2 per mil
d180 latitude gradient for base precipitation: -0.443 per mil/deg lat
Average residence time for falling precipitation: 1409 s
Water-vapor density at sea level: 15.62 g/m^3
Scale height for water vapor: 3008 m
Average velocity for falling precipitation: 2.1
Total density at sea level: 1.21 g/m^3
Scale height for total density: 9734 m
Average lapse-rate ratio, gammaSat/gammaEnv: 0.92

Precipitation State #2:
Moist buoyancy frequency: 0.127 mrad/s
d180 for base precipitation: -2.3 per mil
d180 latitude gradient for base precipitation: -0.554 per mil/deg lat
Average residence time for falling precipitation: 1346 s

Water-vapor density at sea level: 14.19 g/m³
Scale height for water vapor: 2883 m
Average velocity for falling precipitation: 2.1 m/s
Total density at sea level: 1.22 g/m³
Scale height for total density: 9705 m
Average lapse-rate ratio, gammaSat/gammaEnv: 0.92

----- Observed Meteoric Water Line -----
Principal standard deviations (per mil): 0.34, 31.21
Intercept and slope (per mil): 11.09, 8.14

----- Predicted Meteoric Water Line -----
Principal standard deviations (per mil): 0.18, 27.80
Intercept and slope (per mil): 10.9, 8.10

----- Quality of Fit -----
Reduced chi-square: 2.3352
Degrees of freedom: 178
Number of primary samples in wet locations: 197
Number of primary samples: 197
Standard deviation of wet residuals for d2H: 11.2 per mil
Standard deviation of wet residuals for d180: 1.3 per mil
Approximate standard error for predicted d2H: 0.8 per mil
Approximate standard error for predicted d180: 0.1 per mil

----- Computation Time -----
Duration for computation: 0.81 minutes

----- Mat File -----
Results saved in the run directory as mat file:
opiCalc_TwoWinds_Results.mat

Program: opiPairPlots
 Start time: 06-Sep-2022 20:56:39
 Path for solutions file:
 /Users/markbrandon/Dropbox (Yale University)/OPI Mendoza/runs/run043_Mendoza, leeside evaporation, fit for kappa BEST SOLUTION/
 Filename for solutions file:
 08_opiFit_Solutions.txt
 Solutions title:
 run 043, Mendoza area, opi 3.6, two wind, leeside evaporation, fit for kappa

opiPairPlots

Table 1. The parameter constraints used in the search.

Axis Labels	Power-of-10		
	Factors	(Search	Constraints)
1 : U (m/s)	+0	(0.1 , 20)
2 : azimuth	+0	(35 , 145)
3 : T_0 (K)	+0	(270 , 300)
4 : M	+0	(0 , 1.2)
5 : \kappa (km^2/s)	+6	(0 , 1e+06)
6 : \tau_c (s)	+0	(0 , 2500)
7 : \delta^2_0 (%)	-3	(-0.06 , 0)
8 : d\delta^2_0/d\phi (%/°)	-3	(-0.015 , 0)
9 : f_P	+0	(0 , 1)
10: fraction	+0	(0 , 1)
11: U (m/s)	+0	(0.1 , 20)
12: azimuth	+0	(215 , 325)
13: T_0 (K)	+0	(270 , 300)
14: M	+0	(0 , 1.2)
15: \kappa (km^2/s)	+6	(0 , 1e+06)
16: \tau_c (s)	+0	(0 , 2500)
17: \delta^2_0 (%)	-3	(-0.06 , 0)
18: d\delta^2_0/d\phi (%/°)	-3	(-0.015 , 0)
19: f_P	+0	(0 , 1)

Table 2. The best-fit solution and associated univariate 95-percent confidence limits.

Axis Labels	Estimate	(95% Confidence Limit)
1 : U (m/s)	1.95496	(1.91893 , 1.9905)
2 : azimuth	91.3531	(90.9389 , 92.9145)
3 : T_0 (K)	291.215	(291.11 , 291.317)
4 : M	0.0526017	(0.00760984 , 0.0849782)
5 : \kappa (km^2/s)	17.5888	(0.0192824 , 316.157)
6 : \tau_c (s)	0.0285352	(0.000282936 , 23.3462)
7 : \delta^2_0 (%)	-0.015106	(-0.0165921 , -0.014186)
8 : d\delta^2_0/d\phi (%/°)	-0.0036011	(-0.00387564 , -0.00289186)
9 : f_P	0.999887	(0.95372 , 1)
10: fraction	0.289375	(0.253665 , 0.322002)
11: U (m/s)	3.02041	(2.84467 , 3.21676)
12: azimuth	233.228	(232.841 , 233.472)
13: T_0 (K)	289.613	(289.377 , 289.742)
14: M	0.265233	(0.253449 , 0.276767)
15: \kappa (km^2/s)	72479.9	(64855.8 , 79616.1)
16: \tau_c (s)	250.938	(177.531 , 375.262)
17: \delta^2_0 (%)	-0.00788713	(-0.00920856 , -0.00633041)
18: d\delta^2_0/d\phi (%/°)	-0.00450601	(-0.00499308 , -0.00417139)
19: f_P	0.975194	(0.931042 , 0.998222)

----- Background Details about the Search -----

Number of observations for fit: 197

Number of parameters: 19

Number of free parameters: 19

Reduced chi-square for best-fit solution: 2.33505

Degrees of freedom for best-fit solution: 178

Size of solution set: 200

Specified epsilon for stopping criterion, epsilon: 0.0001

Total number of solutions (ignoring nan solutions): 118793

Number of solutions with chiR2==nan: 0

Reduced chi-square for bivariate 95% confidence limit: 2.3687

Number of solutions within bivariate 95% confidence limits: 36716

opiPairPlots, Figure Captions

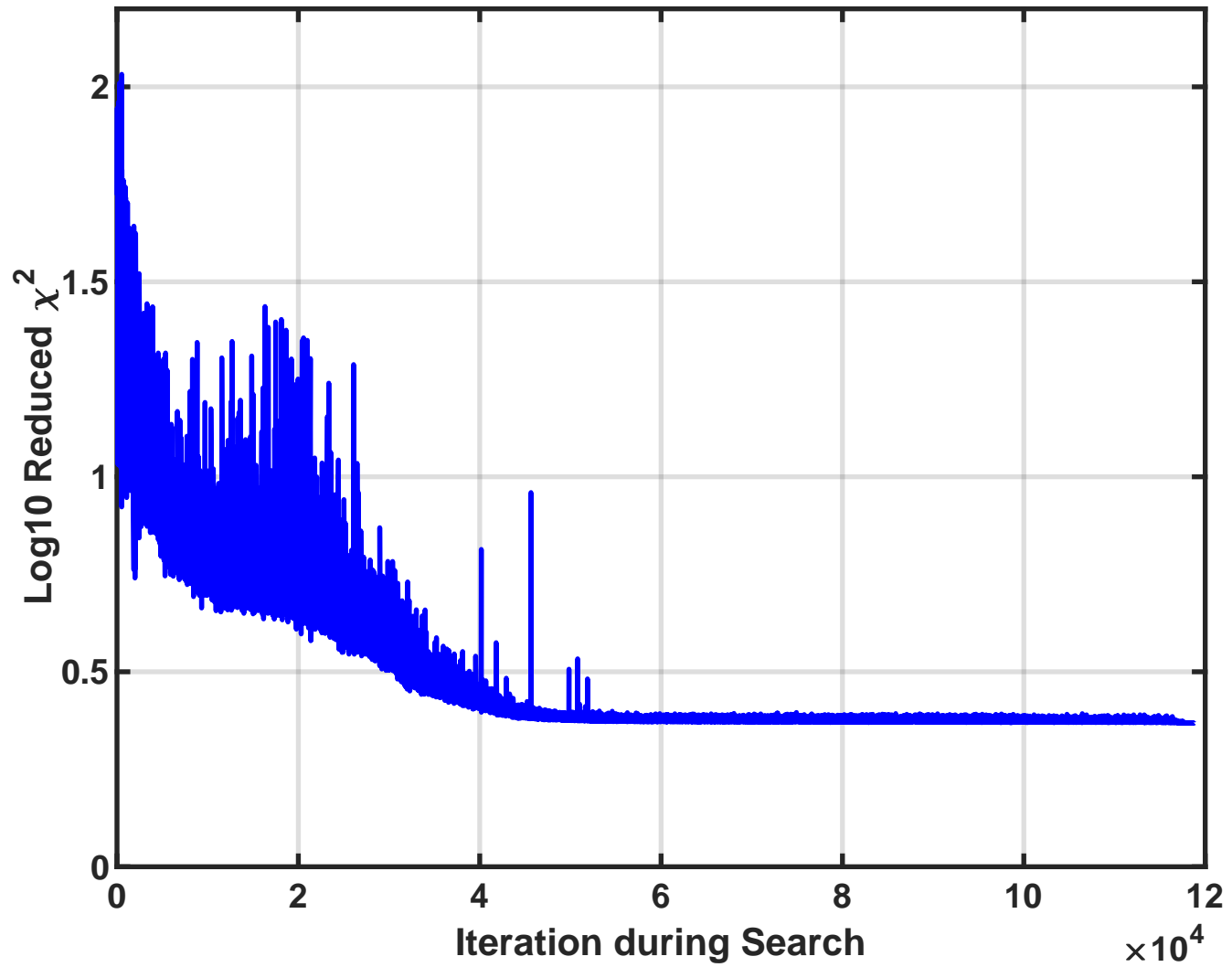
Figure 1. Minimum value of reduced chi-square, χ_r^2 , as a function of the search iteration. The plot shows the evolution and convergence of the search for a best-fit solution.

Figure 2. Termination variable ε as a function of the search iteration. The variable ε is calculated at each step of the search, and is defined by the standard deviation for a set of candidate solutions with the smallest χ_r^2 values. The search is terminated when epsilon is less than a user-specified stopping value, epsilon0 (red line). The solution with the smallest χ_r^2 value at termination is defined as the best-fit solution.

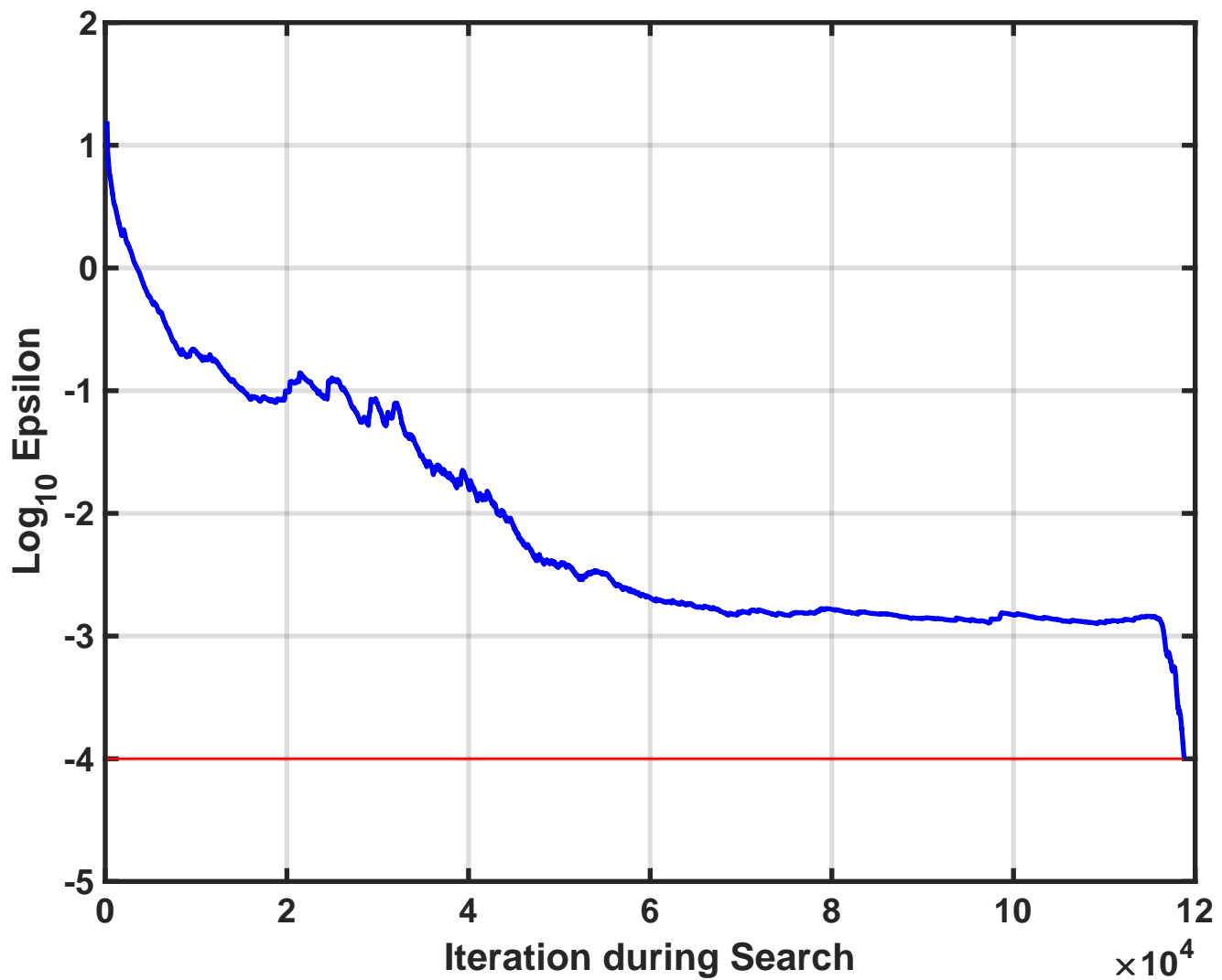
Figure 3. Pair plots showing solutions with χ_r^2 values that lie within the bivariate 95-percent confidence region for each pair of parameters. The selected solutions are projected from the full parameter space into the two-parameter view provided by each plot. The solutions are plotted in order of decreasing χ_r^2 , so that the smallest χ_r^2 solutions are most apparent in the plot. The confidence regions are estimated using the chi2-contour method of Press et al. (2007, p. 812-816).

Figure 4. Pair plot showing χ_r^2 maps for large regions around the best-fit solution, using the same projection and plotting method as described for Figure 3. These plots are helpful for assessing covariance between the parameter estimates, and for judging the convergence of the search and the uniqueness of the best-fit solution.

Fig. 1. Minimum reduced chi-square as function of the search iteration
run 043, Mendoza area, op1 3.6, two wind, leeside evaporation, fit for kappa



**Fig. 2. Termination variable, epsilon, as a function of the search iteration
run 043, Mendoza area, op1 3.6, two wind, leeside evaporation, fit for kappa**



**Figure 3. Confidence limits (95%) for best-fit solution.
run 043, Mendoza area, op1 3.6, two wind, leeside evaporation, fit for kappa**

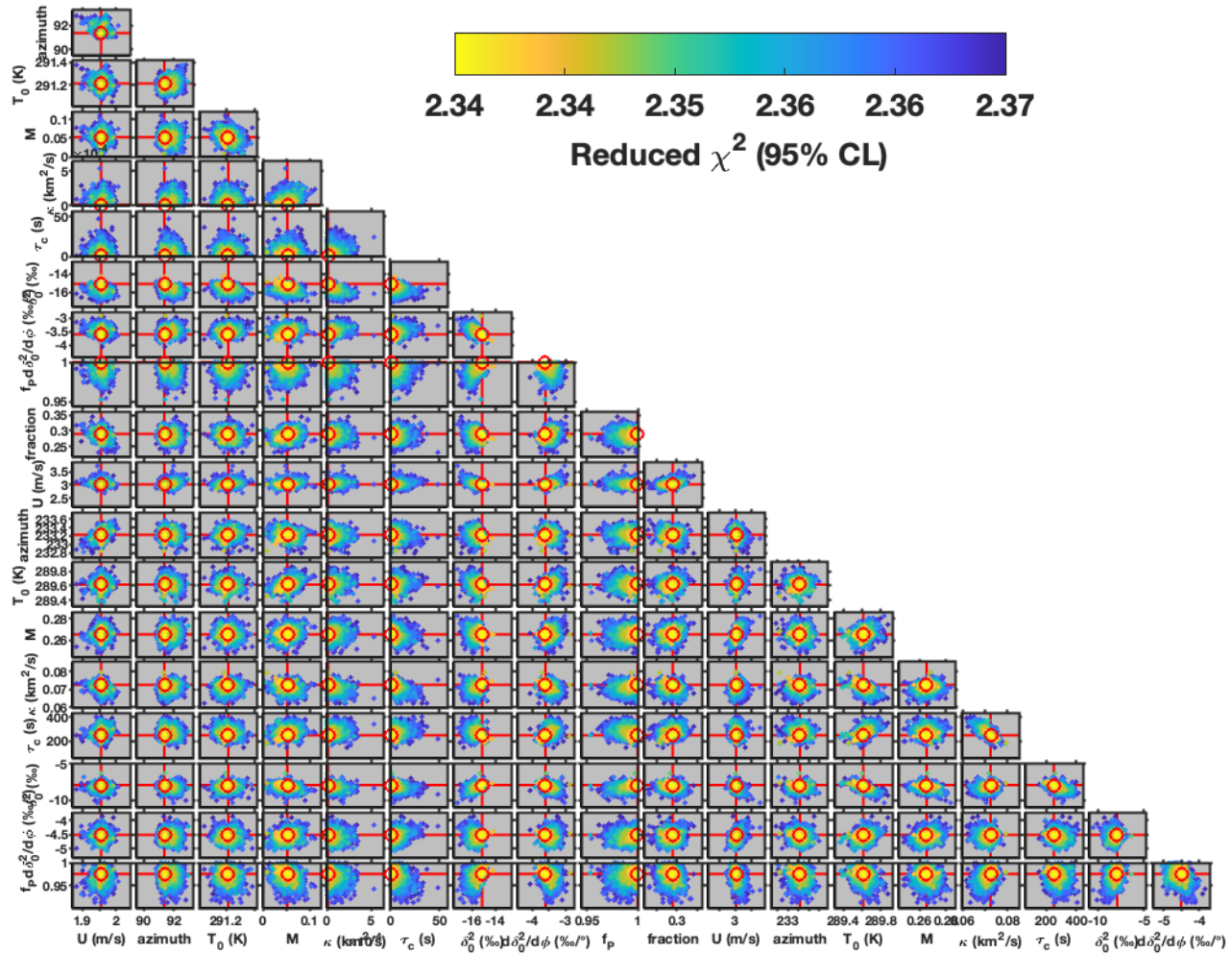
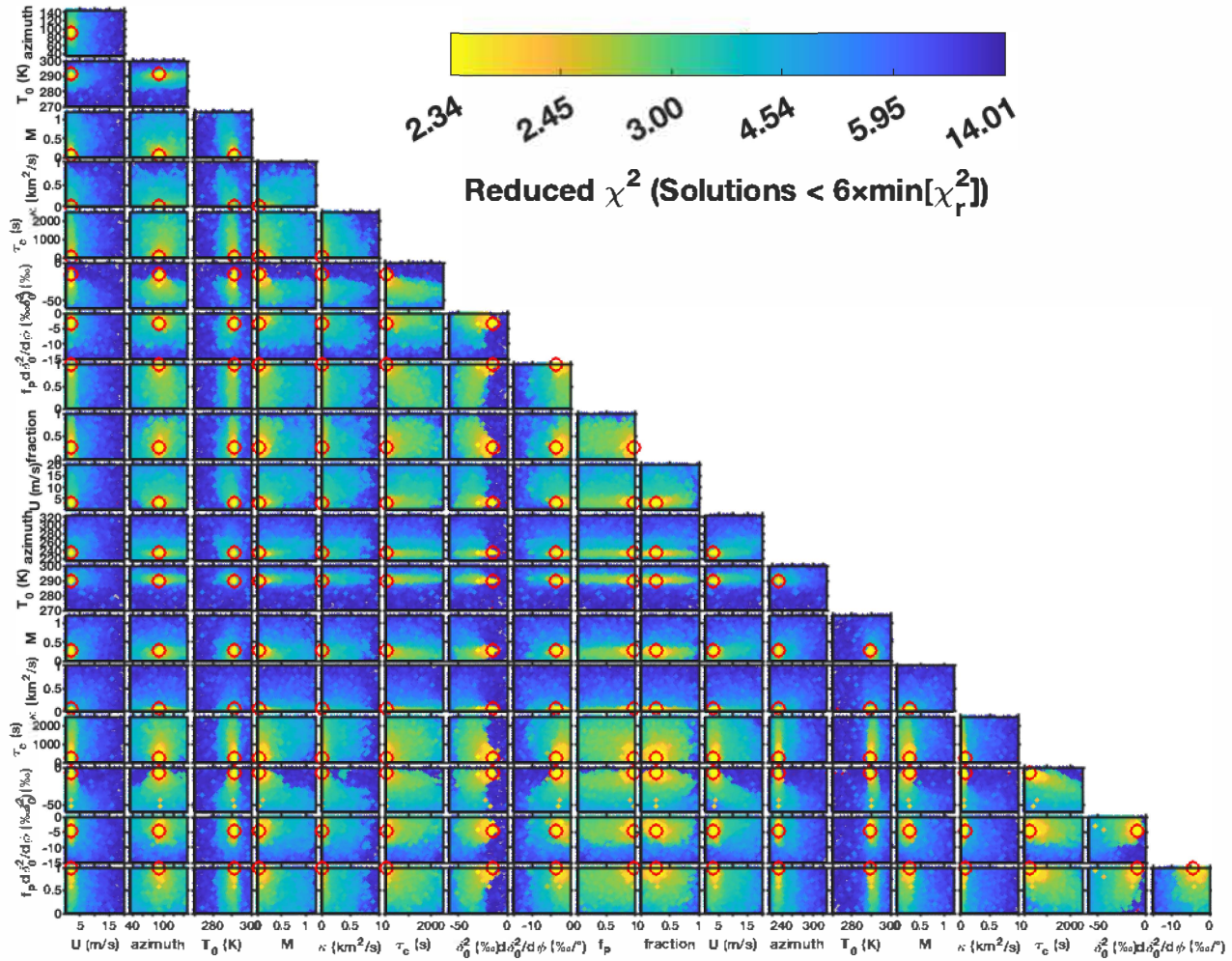


**Figure 4. Maps showing reduced χ^2 around best-fit solution.
run 043, Mendoza area, op1 3.6, two wind, leeside evaporation, fit for kappa**



Program: opiPlots_TwoWinds
Start time: 07-Sep-2022 23:28:47

Run file path:

/Users/markbrandon/Dropbox (Yale University)/OPI Mendoza/runs/run043_Mendoza, leeside evaporation, fit for kappa BEST SOLUTION

Run file name:

run043.run

Run title:

run 043, Mendoza area, opi 3.6, two wind, leeside evaporation, fit for kappa

Path name for data directory:

~/Dropbox/OPI Mendoza/data Mendoza

opiPlots_TwoWinds

----- Topography File -----

Topography file: Mendoza topography_Gebco1km_-85,-43,-42.5,-27.5.mat

Maximum elevation (m): 6318

Grid size, nx and ny: 3827, 1669

Minimum and maximum for longitude: -85.00000, -43.00000 degrees

Minimum and maximum for latitude: -42.50000, -27.50000 degrees

Grid spacing, dLon and dLat (degrees): 0.01098, 0.00899

Grid spacing, dx and dy (km): 1.01, 1.00

Lon, lat for map origin (degrees): -70.24021, -34.38537

Map origin is set to sample centroid.

Size of cosine window as fraction of grid size: 0.25 (dimensionless)

Coriolis frequency at map-origin latitude (mrad/s): -0.082

Lon, lat for section origin (degrees): -69.61000, -35.14000

----- Sample File -----

Sample file: Mendoza area water isotopes (32-38S) 10 Sep 2019.xlsx

Number of all samples: 197

Number of altered samples: 0

Number of primary samples: 197

Number of local primary samples: 3

Number of catchment primary samples: 194

Centroid for primary samples, longitude, latitude: -70.24021, -34.38537 degrees

Minimum and maximum for longitude: -72.09199, -68.07000

Minimum and maximum for latitude: -37.58512, -32.37459

----- Constants -----

Characteristic distance for isotopic exchange (m): 540

Standard-deviation ratio for data residuals: 28.30 (dimensionless)

----- Evaporation Option -----

Evaporative recycling active for both precipitation states.

----- Solution -----

Precipitation State #1:

Wind speed: 2.0 m/s

Azimuth: 91.4 degrees

Sea-level surface-air temperature: 291.2 K (18.1 °C)

Mountain-height number: 0.053 (dimensionless)

Horizontal eddy diffusivity: 17 m^2/s

Average residence time for cloud water: 0 s

d2H for base precipitation: -15.1 per mil

d2H latitude gradient for base precipitation: -3.601 per mil/deg lat

Residual precipitation after evaporation: 1.00 (dimensionless)

Fraction for precipitation state #1: 0.29

Precipitation State #2:

Wind speed: 3.0 m/s

Azimuth: 233.2 degrees

Sea-level surface-air temperature: 289.6 K (16.5 °C)

Mountain-height number: 0.265 (dimensionless)

Horizontal eddy diffusivity: 72558 m^2/s

Average residence time for cloud water: 251 s

d2H for base precipitation: -7.9 per mil

d2H latitude gradient for base precipitation: -4.504 per mil/deg lat

Residual precipitation after evaporation: 0.98 (dimensionless)

---- Other Variables Related to Best-Fit Solution ---

Precipitation State #1:

Moist buoyancy frequency: 0.016 mrad/s

d180 for base precipitation: -3.2 per mil

d180 latitude gradient for base precipitation: -0.443 per mil/deg lat

Average residence time for falling precipitation: 1409 s

Water-vapor density at sea level: 15.62 g/m^3

Scale height for water vapor: 3008 m

Average velocity for falling precipitation: 2.1 m/s

Total density at sea level: 1.21 g/m^3

Scale height for total density: 9734 m

Average lapse-rate ratio, gammaSat/gammaEnv: 0.92 (dimensionless)

Precipitation State #2:

Moist buoyancy frequency: 0.127 mrad/s

d180 for base precipitation: -2.3 per mil

d180 latitude gradient for base precipitation: -0.554 per mil/deg lat

Average residence time for falling precipitation: 1346 s

Water-vapor density at sea level: 14.19 g/m^3

Scale height for water vapor: 2883 m

Average velocity for falling precipitation: 2.1 m/s

Total density at sea level: 1.22 g/m^3

Scale height for total density: 9705 m

Average lapse-rate ratio, gammaSat/gammaEnv: 0.92 (dimensionless)

----- Observed Meteoric Water Line -----

Principal standard deviations (per mil): 0.34, 31.21

Intercept and slope (per mil): 11.09, 8.14

----- Predicted Meteoric Water Line -----

Principal standard deviations (per mil): 0.18, 27.80

Intercept and slope (per mil): 10.9, 8.10

----- Estimates for Lifting Lines-----

The precipitation isotopes are represented using their predicted values from the best-fit OPI solution, either as point estimates if the sample location is designated as "local" (type L), or as the precipitated-weighted value for the upstream catchment if the sample is designated as "catchment" (type C).

The lifting is represented either by elevation or by the maximum lifting along the upwind path. The elevation and maximum lifting are

calculated as either "local" or "catchment" values depending on the designation of the sample (type L or C).

The isotopes are not adjusted for latitudinal gradients (dd2H0_dLat, dd1800_dLat), but this source of error is small and symmetric. The slope of the lines are estimated by least squares but the intercept is held fixed so that it matches the estimated base isotope values (d2H0, d180).

Predicted Isotopes vs Maximum Lifting, State #1

Intercept (per mil) and slope (per mil/km) for d2H: -15.1, -29.0

Intercept (per mil) and slope (per mil/km) for d180: -3.2, -3.6

[-15.1117 -29.0439 -3.22076 -3.59218]

Predicted Isotopes vs Maximum Lifting, State #2

Intercept (per mil) and slope (per mil/km) for d2H: -7.9, -25.6

Intercept (per mil) and slope (per mil/km) for d180: -2.3, -3.2

[-7.88753 -25.5887 -2.3329 -3.18104]

Predicted Isotopes vs Elevation, State #1

Intercept (per mil) and slope (per mil/km) for d2H: -15.1, -29.3

Intercept (per mil) and slope (per mil/km) for d180: -3.2, -3.6

Predicted Isotopes vs Elevation, State #2

Intercept (per mil) and slope (per mil/km) for d2H: -7.9, -24.9

Intercept (per mil) and slope (per mil/km) for d180: -2.3, -3.1

----- Quality of Fit -----

Reduced chi-square: 2.3352

Degrees of freedom: 178

Number of primary samples in wet locations: 197

Number of primary samples: 197

opiPlots_TwoWinds, Figure Caption

Figure 1. Comparison of observed versus predicted isotope values (circles) for samples of primary meteoric water. The predicted values are determined by a least-squares fit of the observed isotopic data to a one-wind OPI model. The fit is considered good if the data follow the 1:1 reference (gray line). The blue and red colors indicate the spatial location of a sample relative to the drainage divide (generically assigned here to side1 and side2, respectively). The blue and red squares indicate the isotopic compositions predicted by OPI for base precipitation derived from winds blowing into side1 and side2, respectively.

Figure 2. Craig plot showing $\delta^2\text{H}$ versus $\delta^{18}\text{O}$ compositions for primary samples. Gray circles mark sample isotope measurements of meteoric water, and the blue and red circles mark the isotopic compositions predicted by the best-fit two-wind solution. The gray line marks the meteoric water line (MWL), as estimated using a total least-squares fit to the sample data. The blue and red squares mark the predicted isotopic composition for base precipitation derived from winds that blow into side1 and side2 of the topography, relative to the drainage divide. The blue and red ellipses are estimated standard-deviation ellipses of the isotopic composition of the base precipitation. This estimated covariance is used to scale the fit of the paired isotopic measurements ($\delta^2\text{H}$ and $\delta^{18}\text{O}$) for each sample location.

Figure 3. Standardized residuals as function of location (easting, northing). These plots are used to assess if the residuals are spatially uncorrelated, which is a fundamental assumption for a least-squares fit. The standardized residual is defined as the difference between the observed and predicted values, divided by the estimated standard error for the observed value. The expectation is that the standardized residuals should have values close to one if the fit is good. The color of the circles, blue and red, once again indicate the location of each sample relative to the drainage divide (side1 versus side2).

Figure 4. Predicted precipitation isotopes (circles) for sample locations versus maximum lifting along the upwind path to each location. Blue and red indicate the location relative to side1 and side2. The lines show estimated linear trends for the data, as separated into blue and red groups. The summary above reports the intercept and slope for each of these estimated "lifting lines". Precipitation isotope data typically show a tighter linear relationship with respect to maximum lifting, as opposed to local elevation (see figure 4 for comparison).

Figure 5. Predicted precipitation isotopes as a function of local elevation. The layout is the same as for figure 4.

Fig. 1. Observed versus predicted isotope values

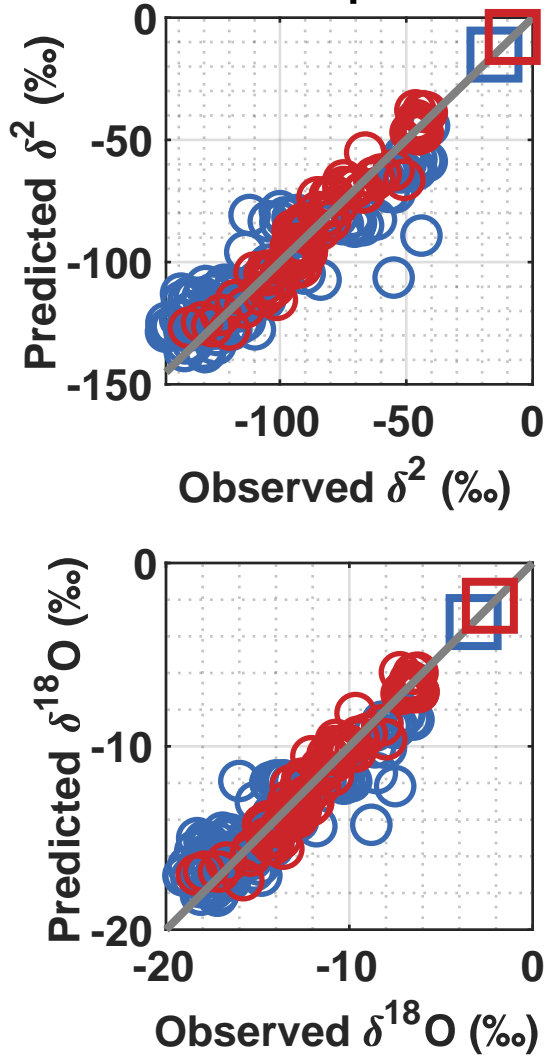


Fig. 2. Craig plot of primary samples

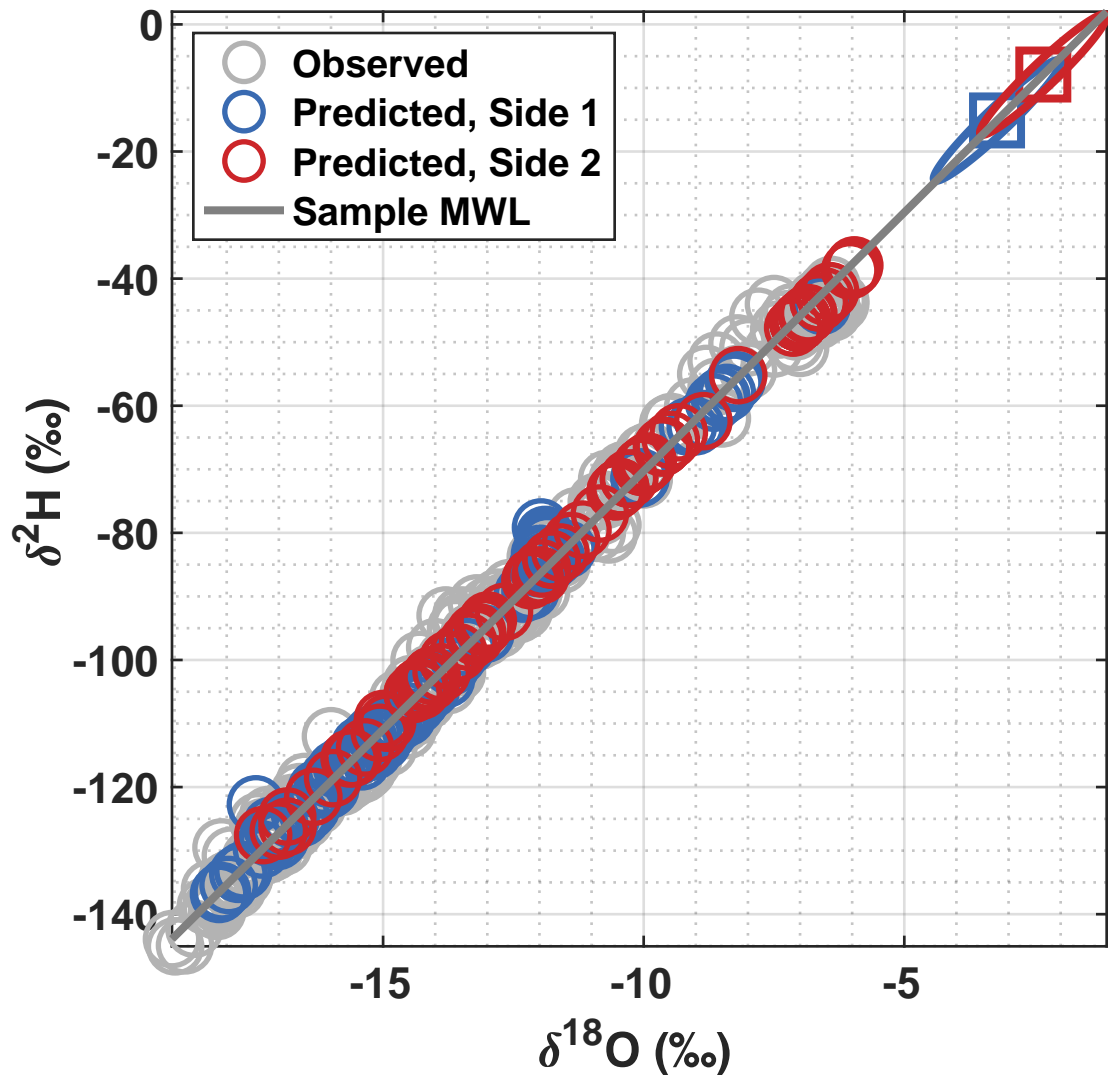


Fig. 3. Standardized residuals for best-fit solution

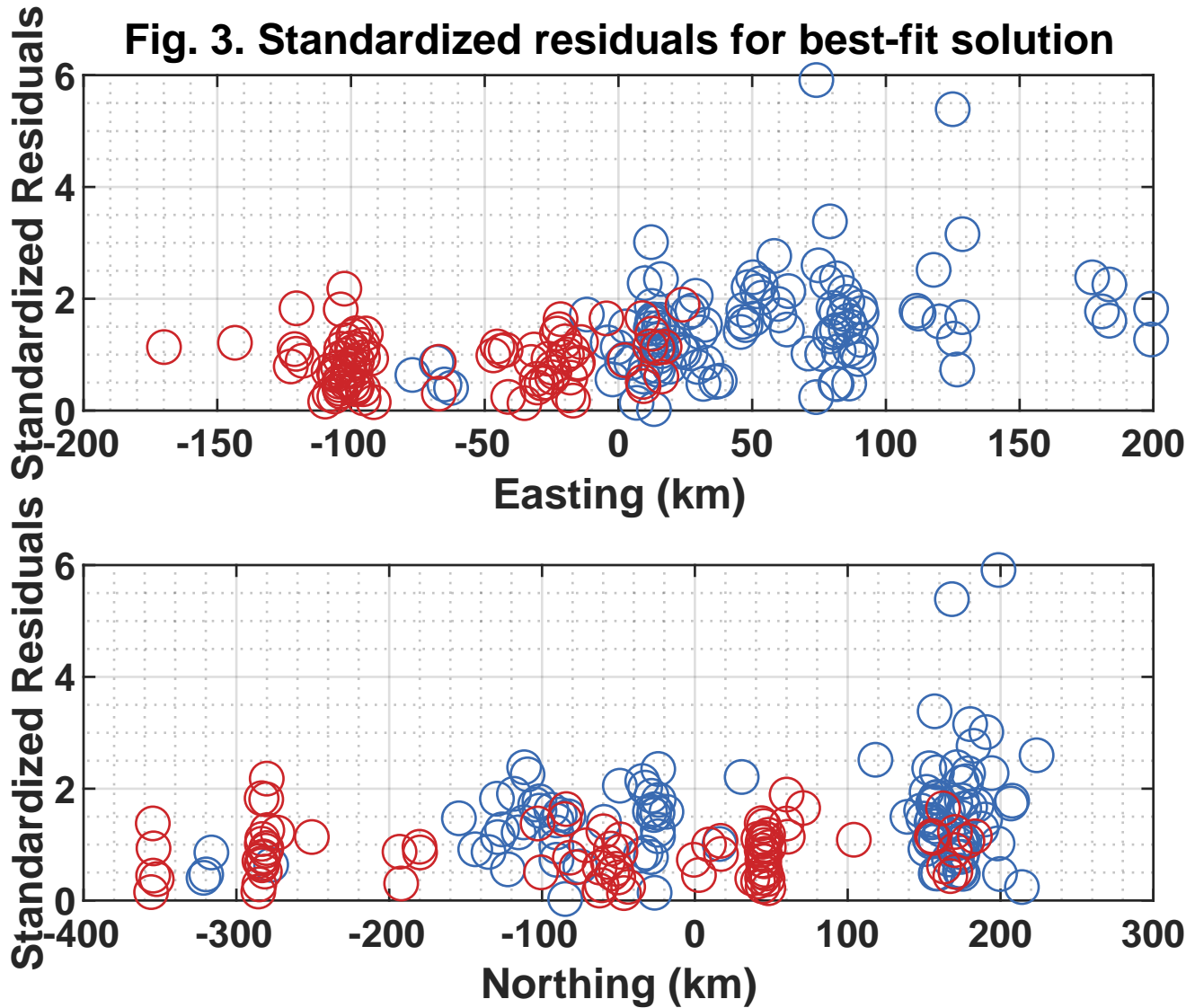


Fig. 4. Predicted isotopes versus maximum lifting

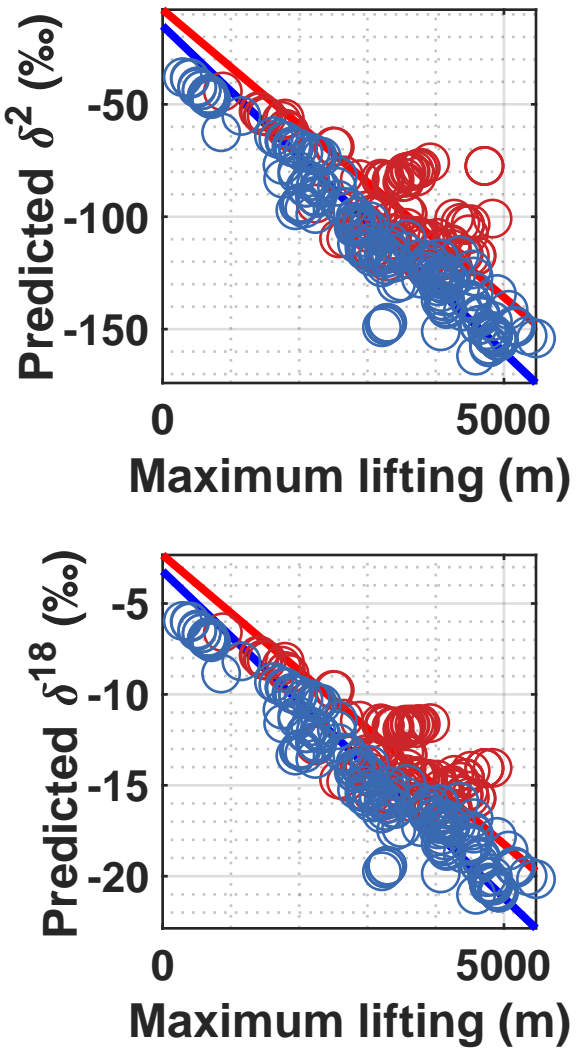
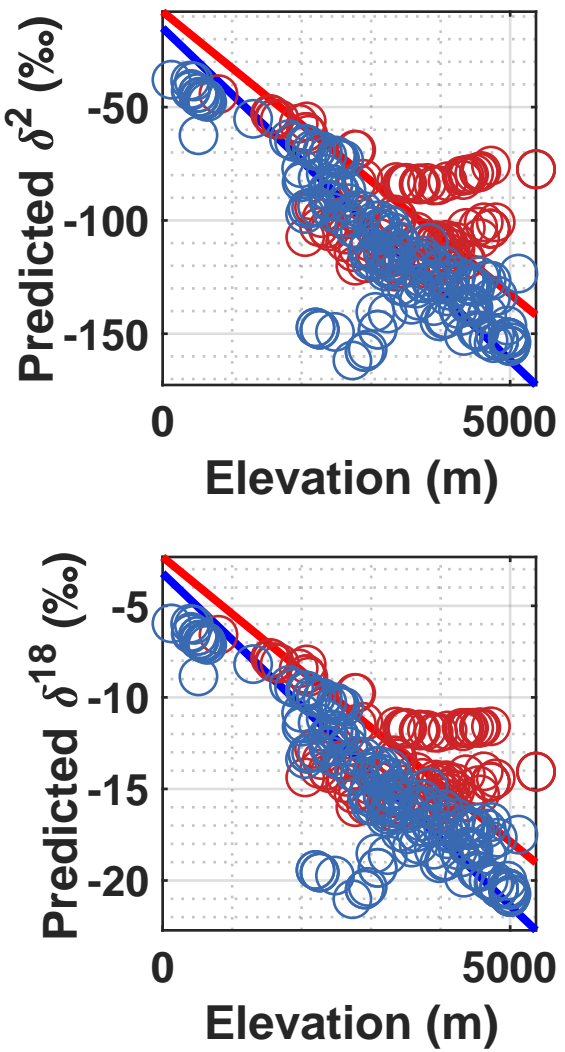


Fig. 5. Predicted isotopes versus elevation



Program: opiMaps_TwoWinds
Start time: 07-Sep-2022 23:29:10

opiMaps_TwoWinds

Run file path:

/Users/markbrandon/Dropbox (Yale University)/OPI Mendoza/runs/run043_Mendoza, leeside evaporation, fit for kappa BEST SOLUTION

Run file name:

run043.run

Run title:

run 043, Mendoza area, opi 3.6, two wind, leeside evaporation, fit for kappa

Path name for data directory:

~/Dropbox/OPI Mendoza/data Mendoza

----- Topography File -----

Topography file: Mendoza topography_Gebco1km_-85,-43,-42.5,-27.5.mat

Maximum elevation: 6318 m

Grid size, nx and ny: 3827, 1669

Longitude, minimum and maximum: -85.00000, -43.00000 degrees

Latitude, minimum and maximum: -42.50000, -27.50000 degrees

Grid spacing, dLon and dLat: 0.01098, 0.00899 degrees

Grid spacing, dx and dy: 1.01, 1.00 km

User-defined map limits, longitude: -75.00000, -63.00000

User-defined map limits, latitude: -39.00000, -31.00000

Continental-divide file: Mendoza_contDivideLonLat.mat

Lon, lat for map origin (degrees): -70.24021, -34.38537

Map origin is set to sample centroid.

Size of cosine window as fraction of grid size: 0.25

Coriolis frequency at map-origin latitude: -0.08237 mrad/s

Lon, lat for section origin (degrees): -69.61000, -35.14000

----- Sample File -----

Sample file: Mendoza area water isotopes (32-38S) 10 Sep 2019.xlsx

Number of all samples: 197

Number of altered samples: 0

Number of primary samples: 197

Number of local primary samples: 3

Number of catchment primary samples: 194

Centroid for primary samples, longitude, latitude: -70.24021, -34.38537 degrees

Minimum and maximum for longitude: -72.09199, -68.07000

Minimum and maximum for latitude: -37.58512, -32.37459

----- Constants -----

Characteristic distance for isotopic exchange: 540 m

Standard-deviation ratio for data residuals: 28.30 (dimensionless)

----- Evaporation Option -----

Evaporative recycling active for both precipitation states.

----- Solution -----

Precipitation State #1:

Wind speed: 2.0 m/s

Azimuth: 91.4 degrees

Sea-level surface-air temperature: 291.2 K (18.1 °C)

Mountain-height number: 0.053 (dimensionless)

Horizontal eddy diffusivity: 17 m^2/s

Average residence time for cloud water: 0 s

d2H for base precipitation: -15.1 per mil

d2H latitude gradient for base precipitation: -3.601 per mil/deg lat
Residual precipitation after evaporation: 1.00 (dimensionless)
Fraction for precipitation state #1: 0.29

Precipitation State #2:

Wind speed: 3.0 m/s
Azimuth: 233.2 degrees
Sea-level surface-air temperature: 289.6 K (16.5 °C)
Mountain-height number: 0.265 (dimensionless)
Horizontal eddy diffusivity: 72558 m^2/s
Average residence time for cloud water: 251 s
d2H for base precipitation: -7.9 per mil
d2H latitude gradient for base precipitation: -4.504 per mil/deg lat
Residual precipitation after evaporation: 0.98 (dimensionless)

---- Other Variables Related to Best-Fit Solution ---

Precipitation State #1:

Moist buoyancy frequency: 0.016 mrad/s
d180 for base precipitation: -3.2 per mil
d180 latitude gradient for base precipitation: -0.443 per mil/deg lat
Average residence time for falling precipitation: 1409 s
Water-vapor density at sea level: 15.62 g/m^3
Scale height for water vapor: 3008 m
Average velocity for falling precipitation: 2.1 m/s
Total density at sea level: 1.21 g/m^3
Scale height for total density: 9734 m
Average lapse-rate ratio, gammaSat/gammaEnv: 0.92 (dimensionless)

Precipitation State #2:

Moist buoyancy frequency: 0.127 mrad/s
d180 for base precipitation: -2.3 per mil
d180 latitude gradient for base precipitation: -0.554 per mil/deg lat
Average residence time for falling precipitation: 1346 s
Water-vapor density at sea level: 14.19 g/m^3
Scale height for water vapor: 2883 m
Average velocity for falling precipitation: 2.1 m/s
Total density at sea level: 1.22 g/m^3
Scale height for total density: 9705 m
Average lapse-rate ratio, gammaSat/gammaEnv: 0.92 (dimensionless)

----- Streamlines and Cloud Water -----

Vertical exaggeration for streamline figure: 20000 (dimensionless)
Starting elevation for streamlines: 2000 m
Precipitation State 1:
Mean height (above ground surface) for cloud water: 2675 m
Precipitation State 2:
Mean height (above ground surface) for cloud water: 2321 m
Compute time: 7.10 minutes

opiMaps_TwoWinds, Figure Captions

Figure 1. Topography and sample locations (black circles). Blue and red arrows show wind directions for precipitation states #1 and #2, respectively. Red outlines show upslope catchments for catchment samples. Black square marks the user-defined origin for the cross sections. The red line indicates the drainage divide (if provided by the user).

Figure 2. Predicted mean orographic precipitation rate (mm/h), as indicated by a two-winds OPI solution, with both precipitation states combined. White regions indicate no precipitation.

Figure 3. Predicted streamlines (red lines) for atmospheric flow associated with precipitation state #1. The streamlines start at an elevation of 2000 m at the upwind limit of the model domain.

Figure 4. Predicted streamlines (red lines) for atmospheric flow associated with precipitation state #2. The streamlines start at an elevation of 2000 m at the upwind limit of the model domain.

Figure 5. Cross section of precipitation state #1. Top panel shows topography (brown), air flow (black streamlines), cloud-water distribution (gray), and precipitation fall lines (dotted black lines). The Wegener-Bergeron-Findeisen (WBR) zone is delimited by the two blue lines, and marks the upward transition in the atmosphere from rain to ice. The center panel shows the predicted orographic precipitation. The bottom panel shows the predicted distribution of $\delta^2\text{H}$ in precipitation. The dashed line shows the $\delta^2\text{H}$ composition of base precipitation, which includes an estimated latitudinal gradient. The section is oriented in the state #1 wind direction. The section is parallel to the wind direction, and the origin is set at a user-specified location.

Figure 6. Cross section for precipitation state #2. See figure 5 for details.

Figure 7. Predicted $\delta^2\text{H}$ for orographic precipitation with both states combined. White regions indicate no precipitation.

Figure 8. Predicted $\delta^{18}\text{O}$ for orographic precipitation with both states combined. White regions indicate no precipitation.

Figure 9. Mix of orographic precipitation sources, which is shown as the fraction of state #1 precipitation relative to the total predicted orographic precipitation. White regions indicate no precipitation.

Figure 10. Predicted orographic precipitation rate (mm/h) for precipitation state #1. White regions indicate no precipitation.

Figure 11. Predicted orographic precipitation rate (mm/h) for precipitation state #2. White regions indicate no precipitation.

Figure 12. Predicted moisture ratio for precipitation state #1. The atmosphere starts with a moisture ratio of one at the upwind limit of the model domain.

Figure 13. Predicted moisture ratio for precipitation state #2. See figure 12 for details.

Figure 14. Predicted δ^2H for precipitation associated with state #1.

Figure 15. Predicted δ^2H for precipitation associated with state #2.

Figure 16. Surface temperature for precipitation state #1.

Figure 17. Surface temperature for precipitation state #2.

Figure 18. Surface velocity ratio, u'/U , for precipitation state #1, where U is the mean wind speed, and u' is the perturbation in wind speed relative to the mean for a location at the topographic surface. This map is useful for assessing if the solution is consistent with the linear approximation used to calculate the wind velocity field, and if there are areas with significant blocking. The linear approximation requires that $|u'/U| < 1$, and blocking is indicated when $u'/U > 1$.

Figure 19. Surface velocity ratio, u'/U , for precipitation state #2. See figure 18 for details.

Figure 20. Location of outlier samples. The blue points show all sample locations. Standardized residuals are reported adjacent to those samples that have large misfits (standardized residuals > 3) relative to the best-fit solution.

Fig. 1. Topography and sample locations

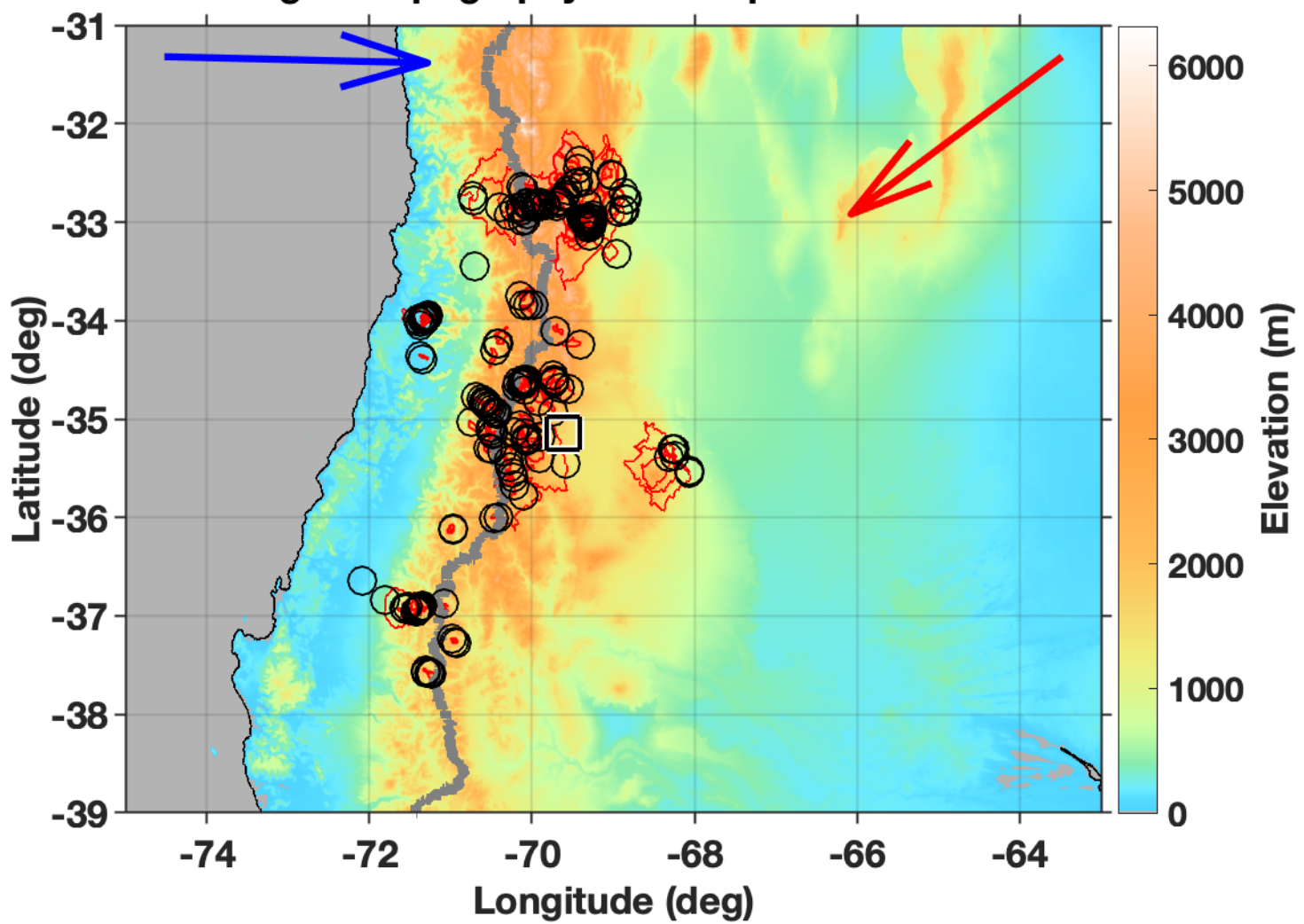


Fig. 2. Precipitation rate

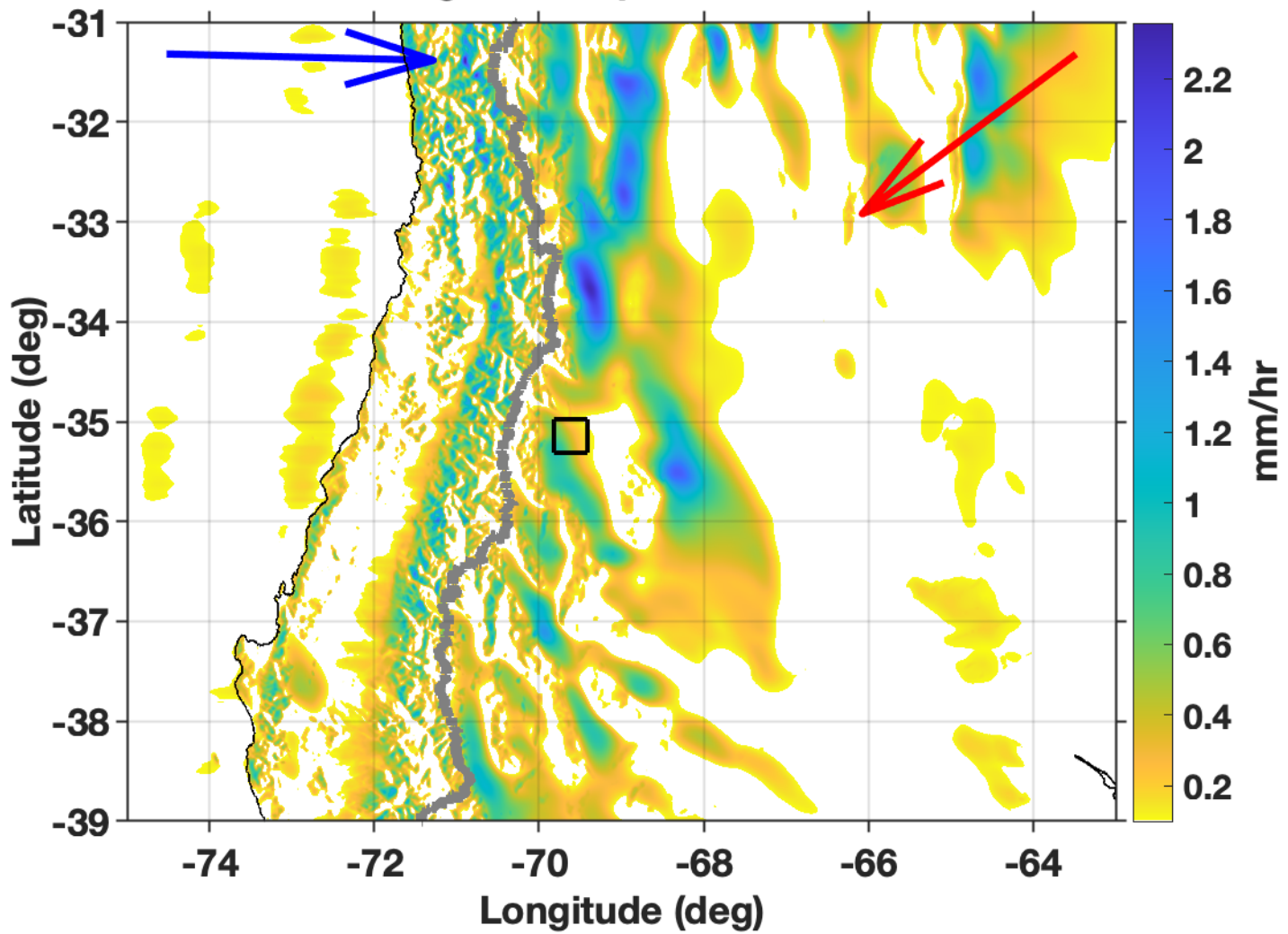


Fig. 3. Streamlines for precipitation state #1

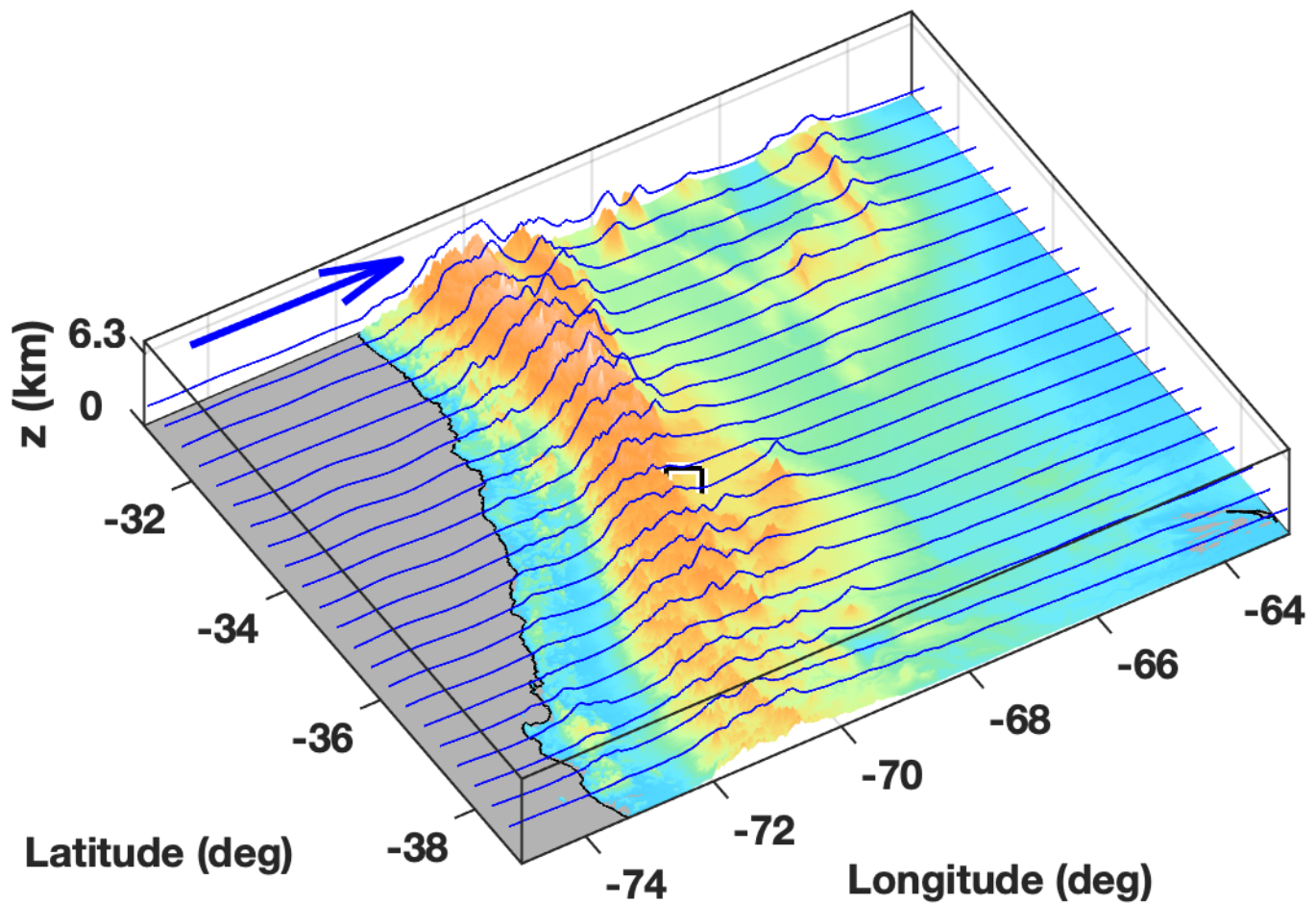


Fig. 4. Streamlines for precipitation state #2

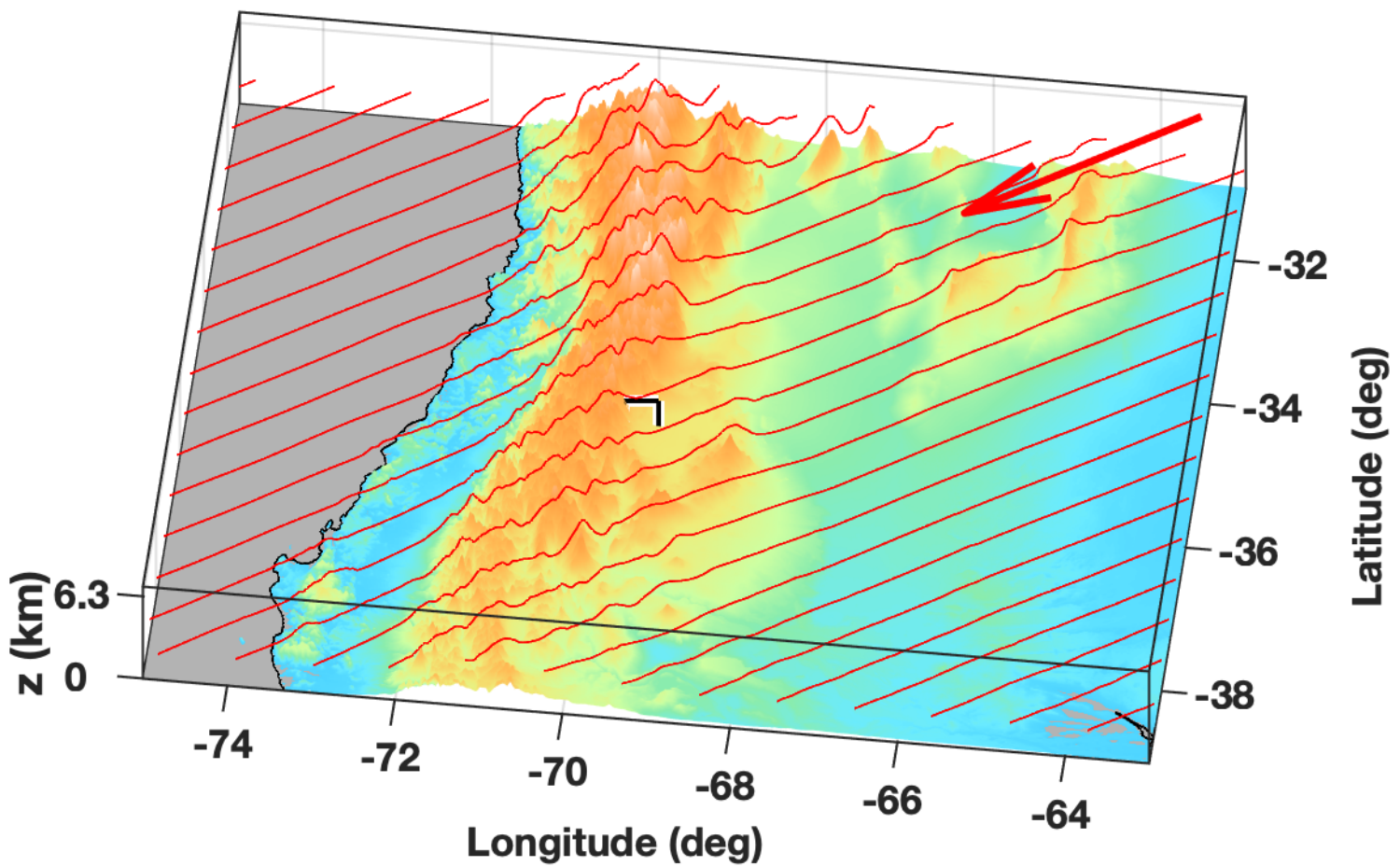


Fig. 5. Cross section for precipitation state #1

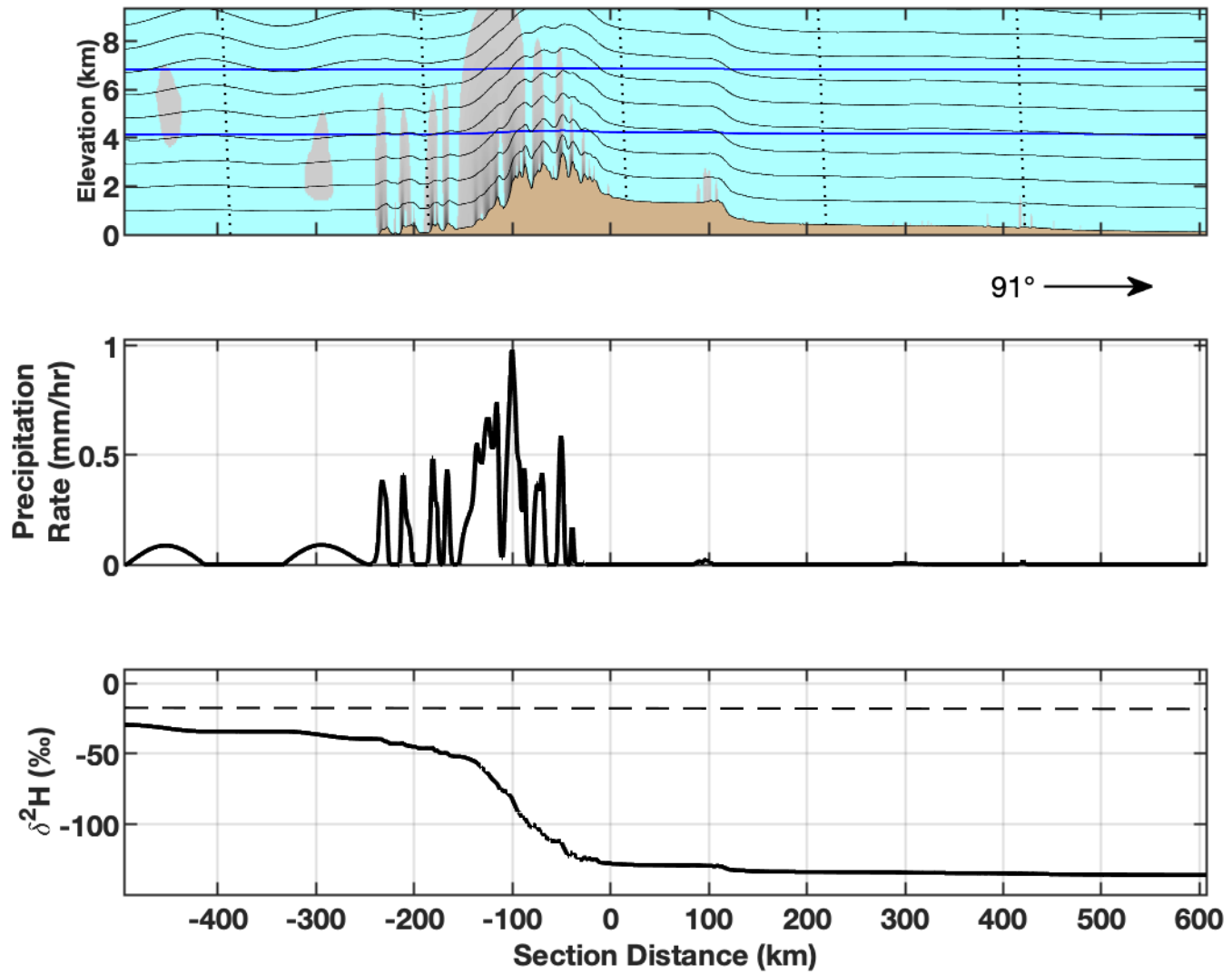


Fig. 6. Cross section for precipitation state #2

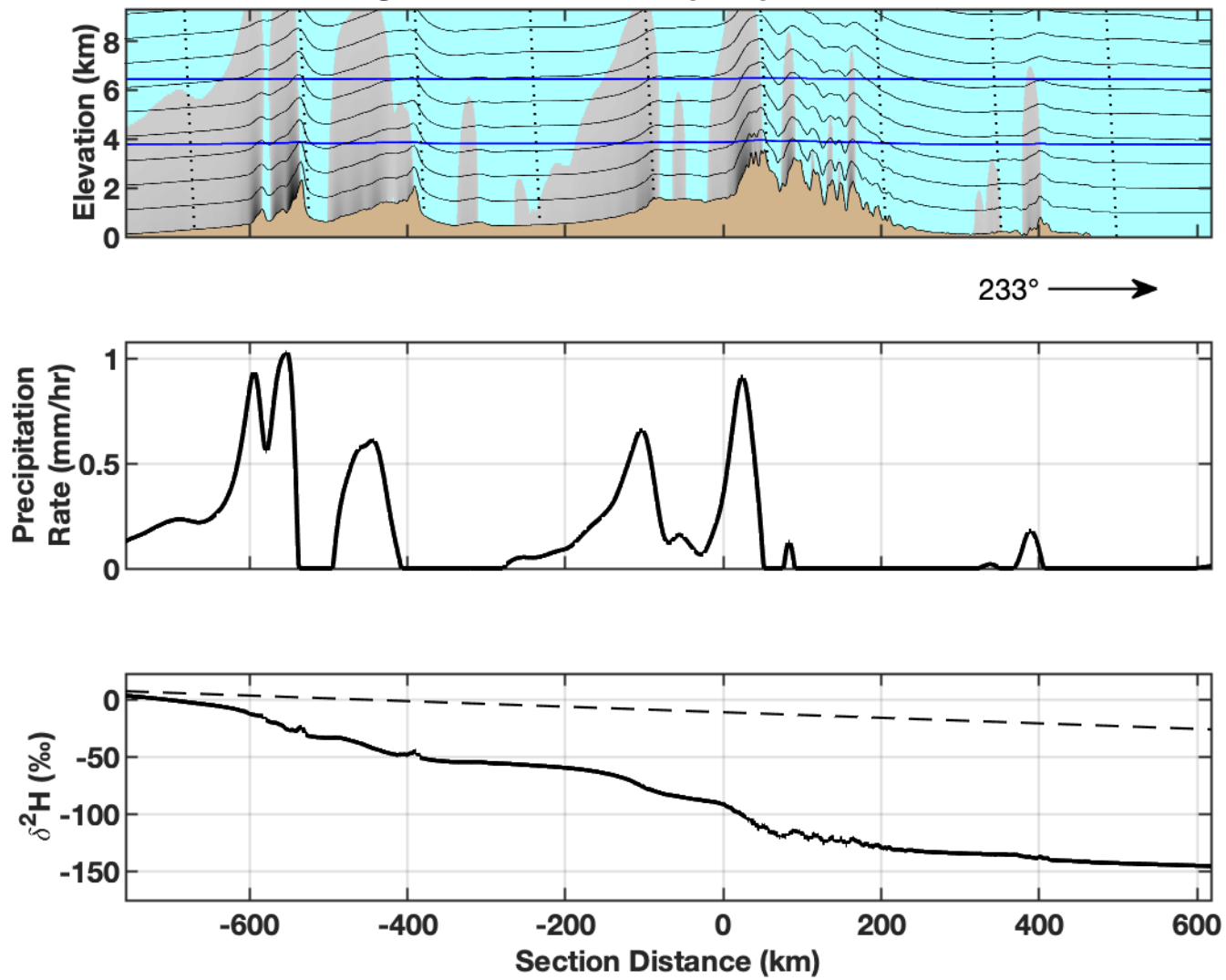


Fig. 7. Predicted precipitation $\delta^2\text{H}$

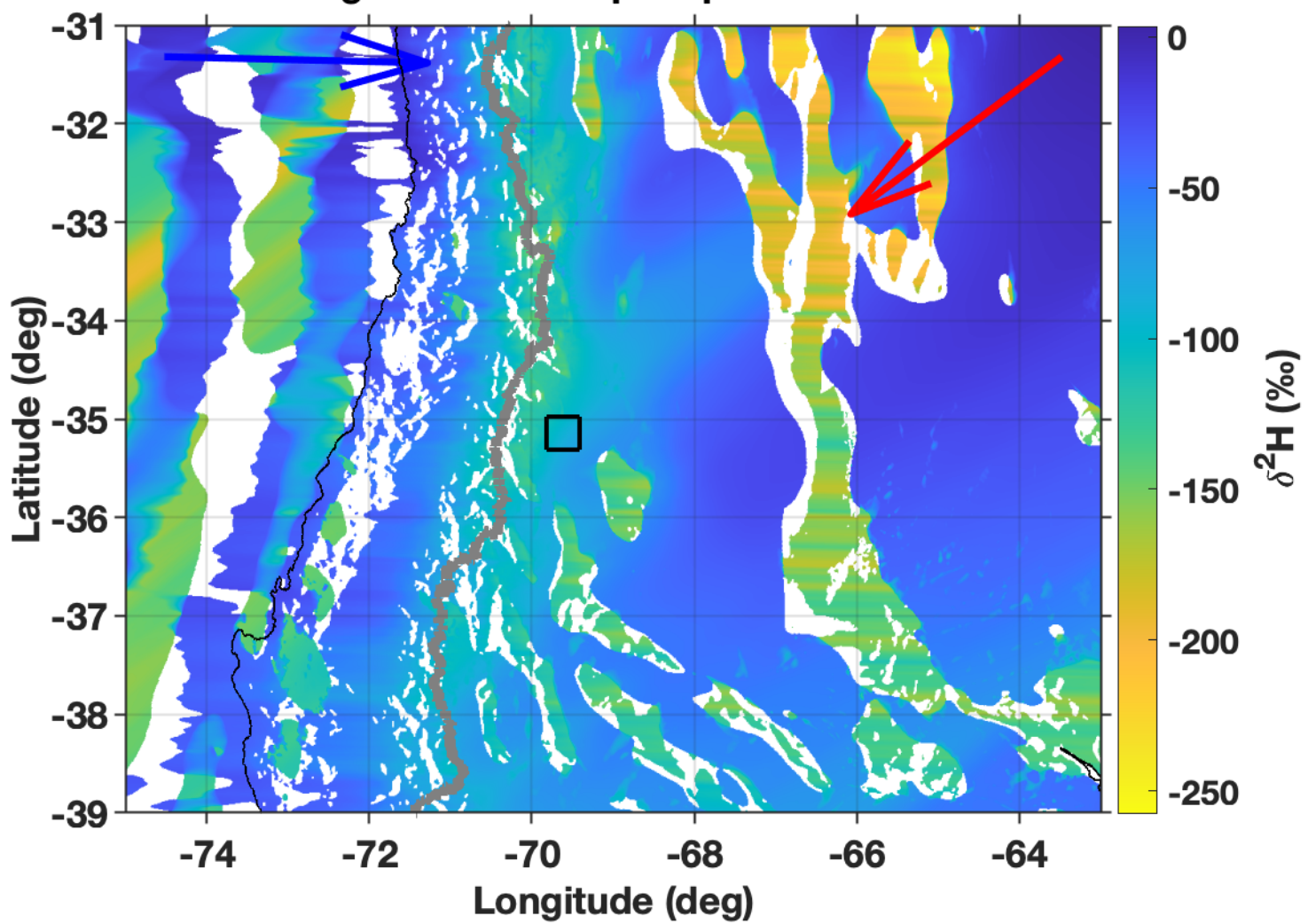


Fig. 8. Predicted precipitation $\delta^{18}\text{O}$

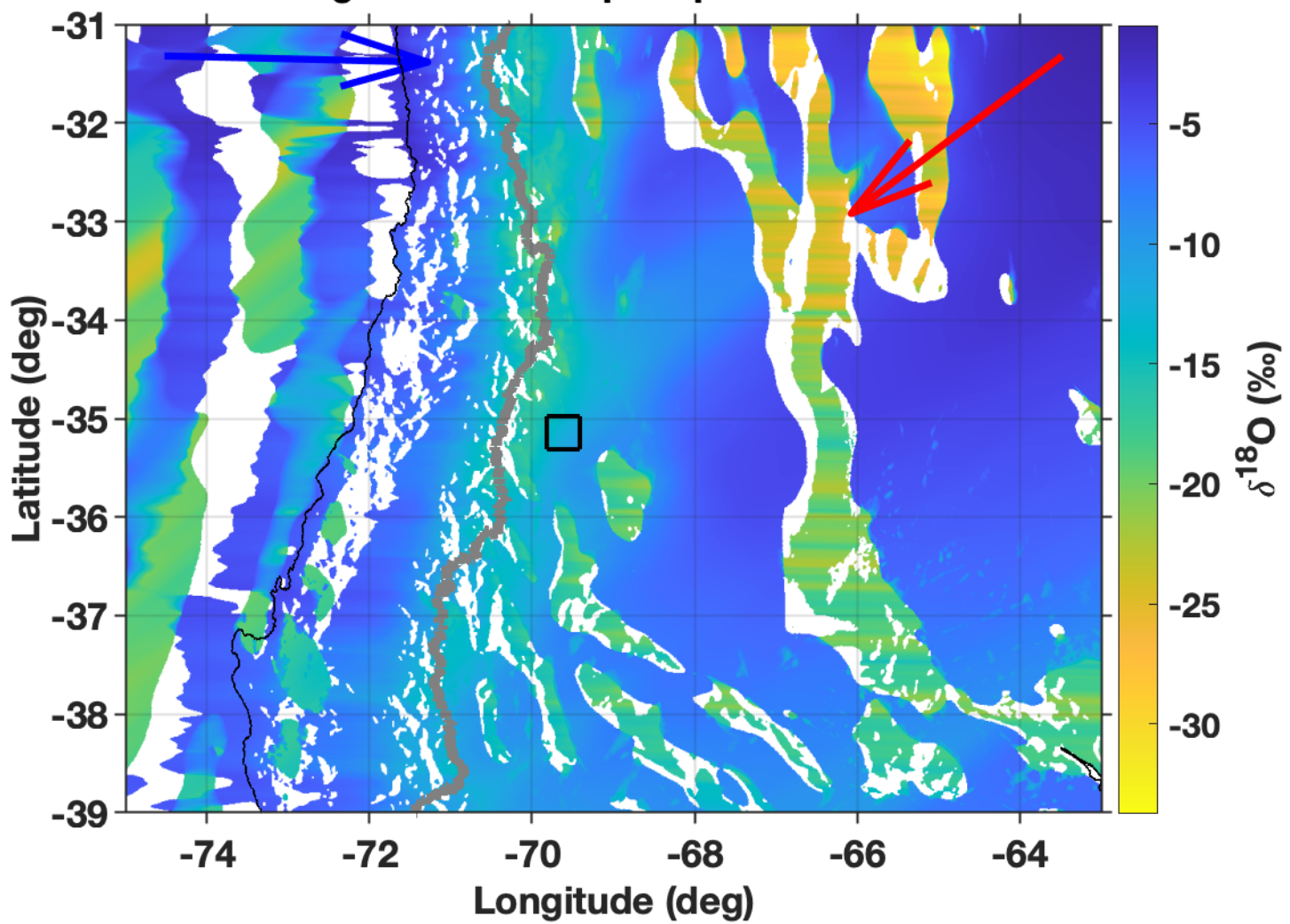


Fig. 9. Precipitation source

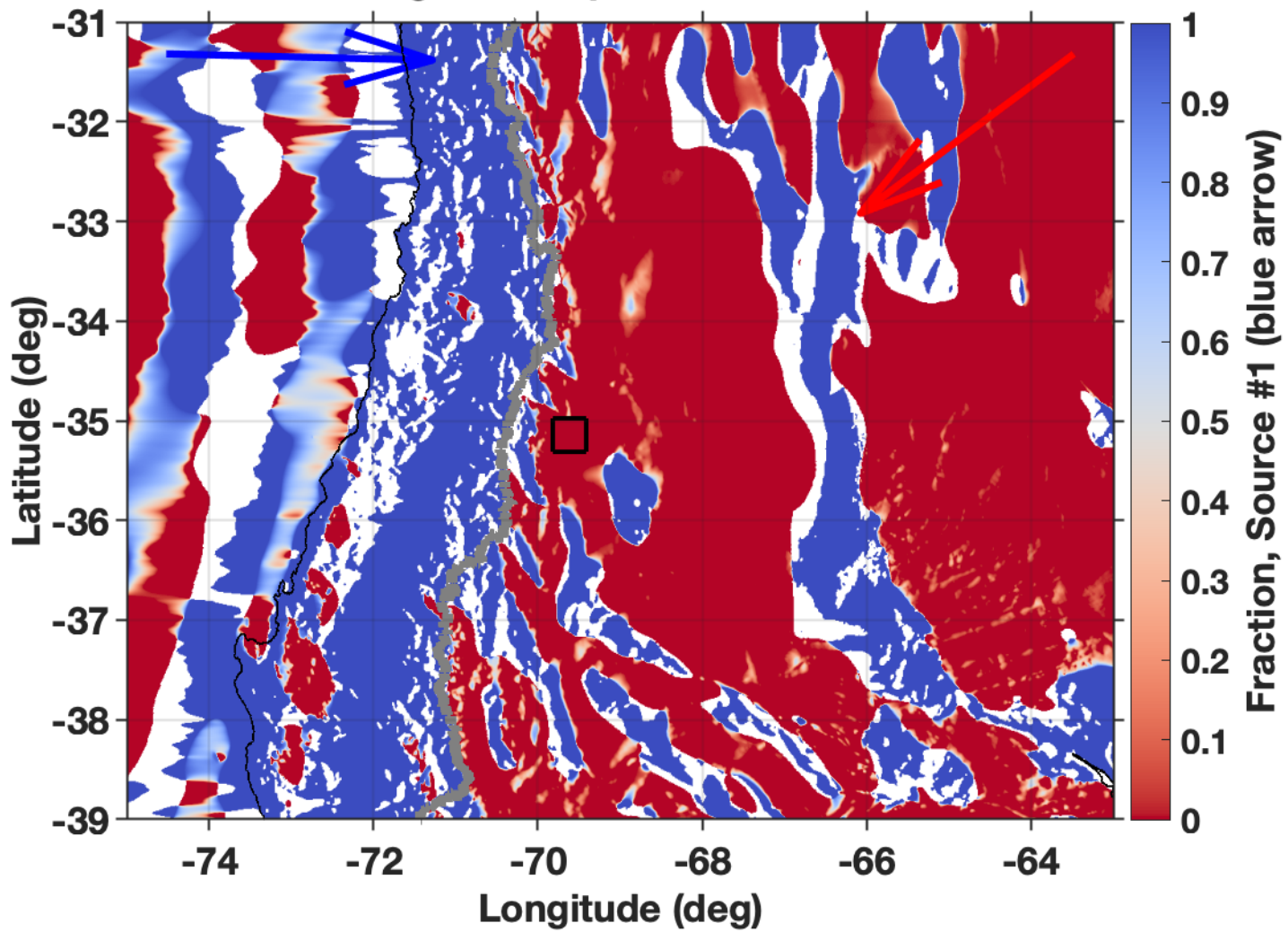


Fig. 10. Precipitation rate, state #1

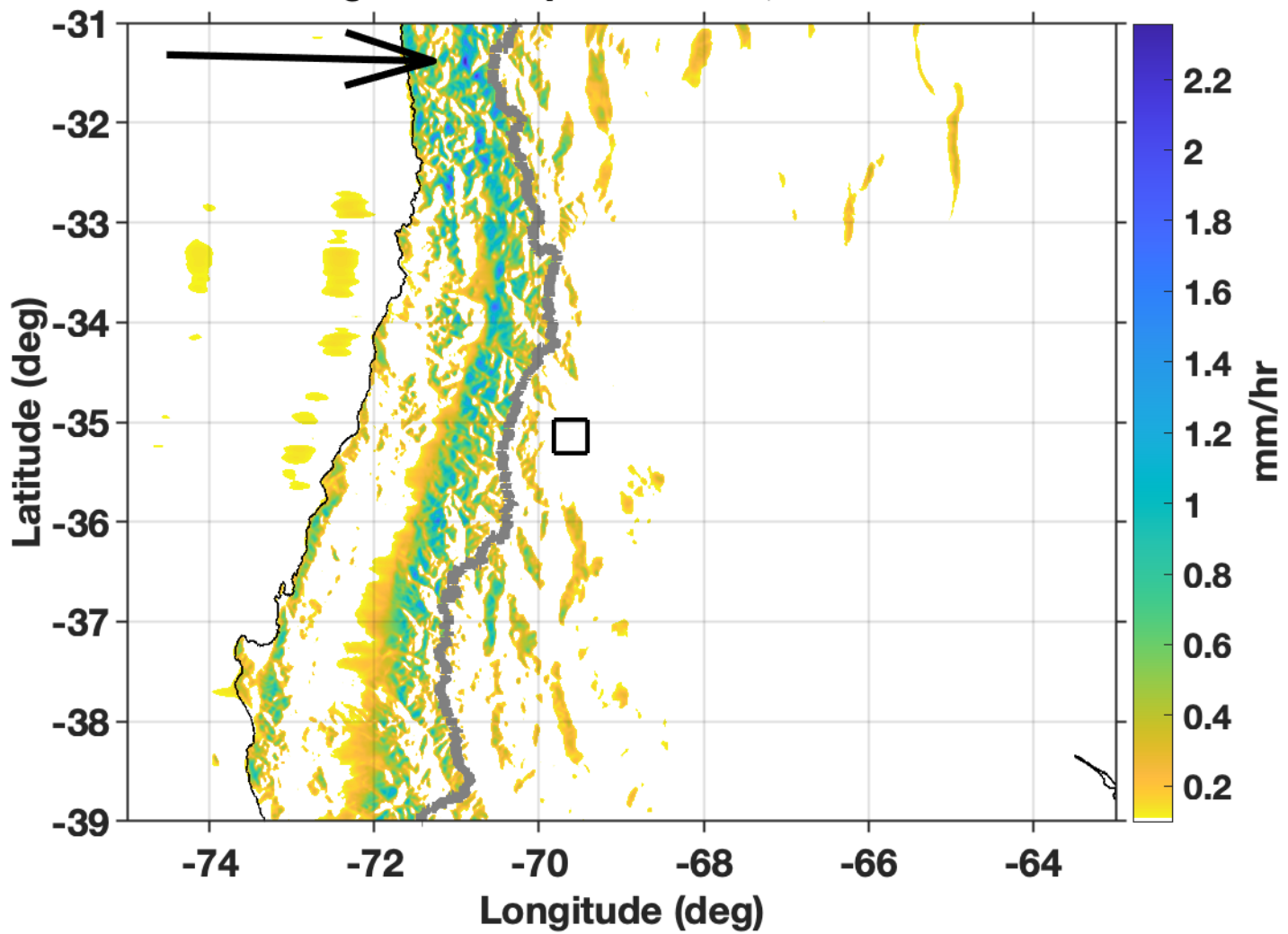


Fig. 11. Precipitation rate, state #2

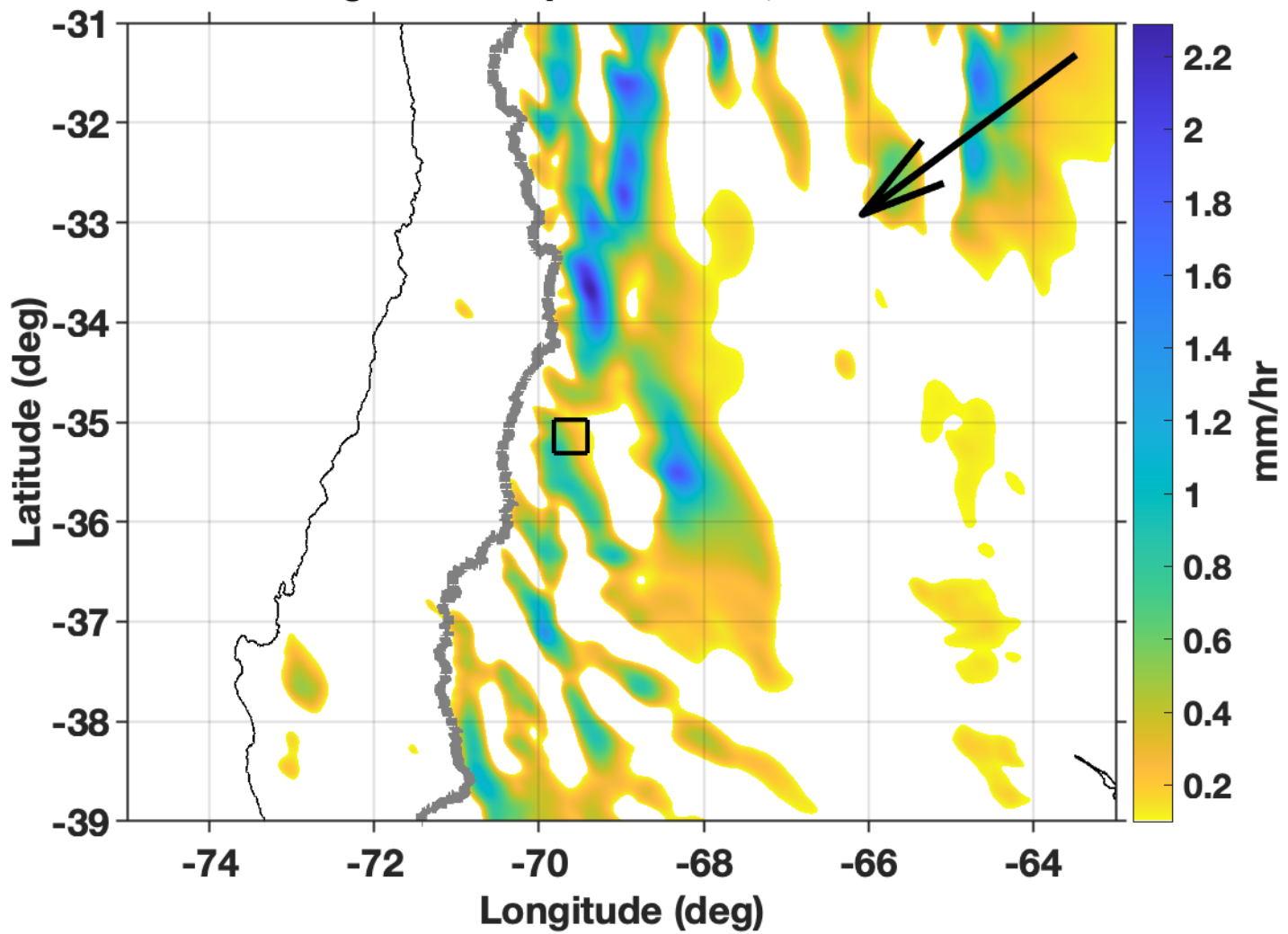


Fig. 12. Moisture ratio, state #1

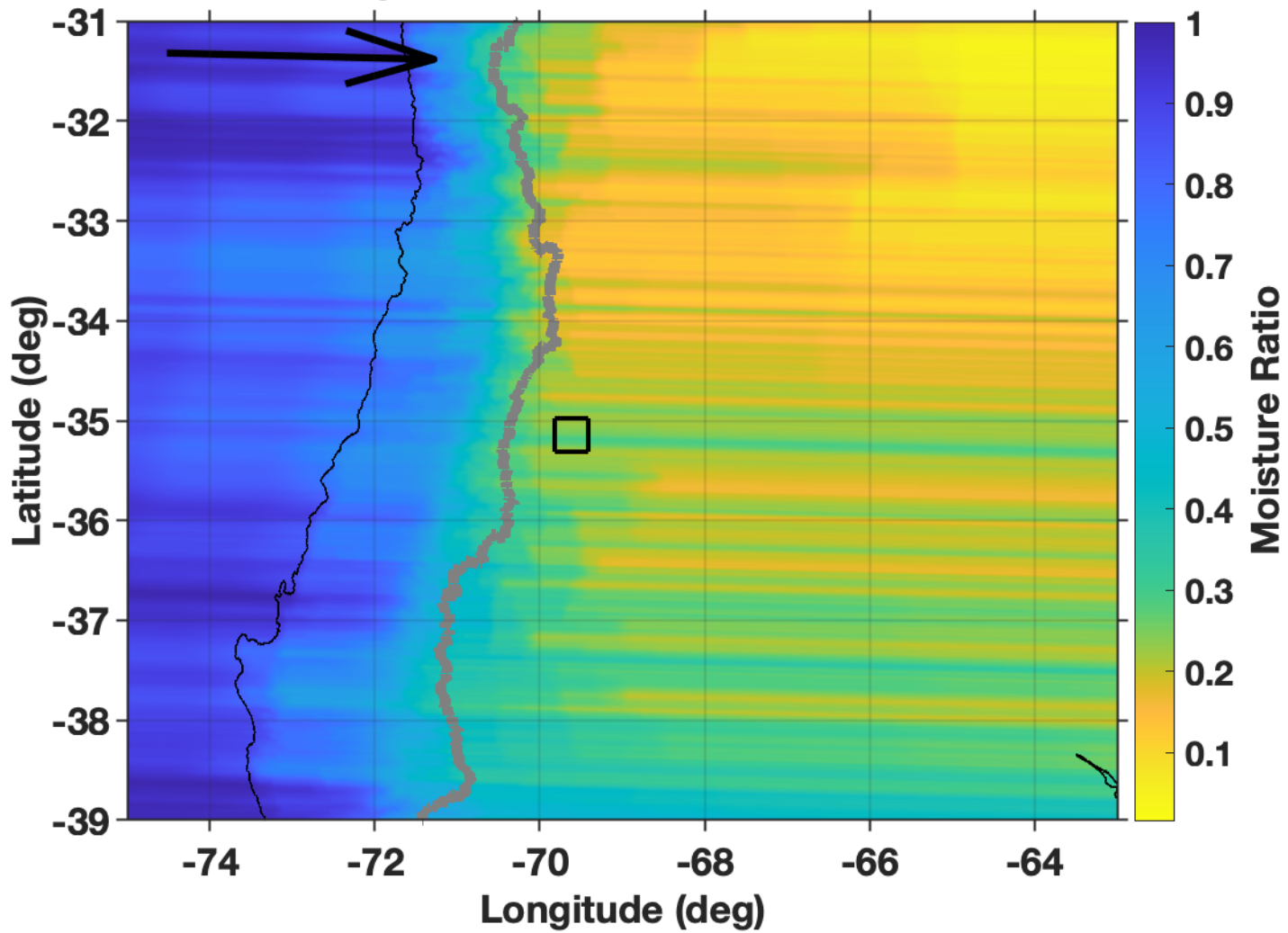


Fig. 13. Moisture ratio, state #2

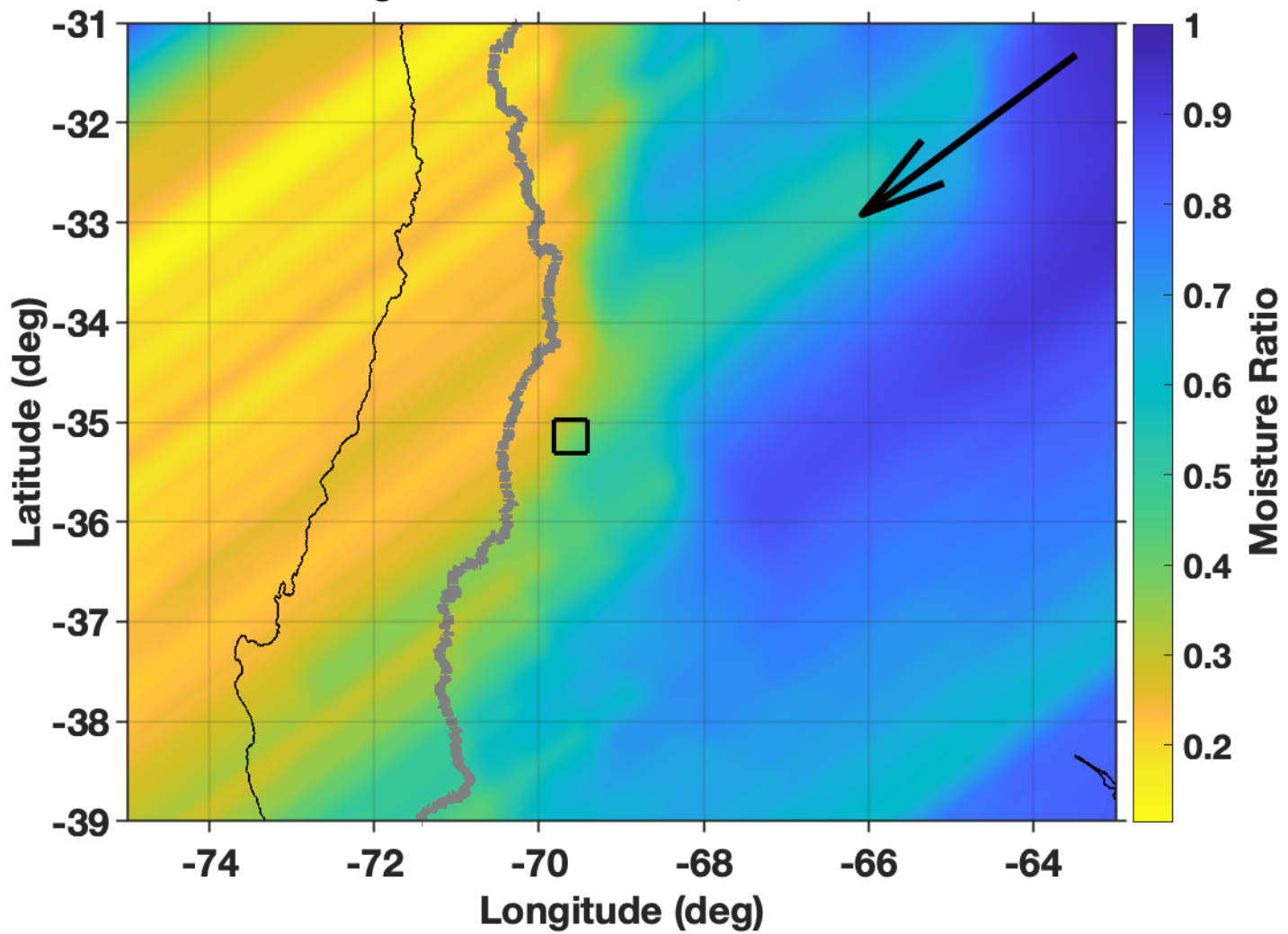


Fig. 14. Predicted precipitation $\delta^2\text{H}$, state #1

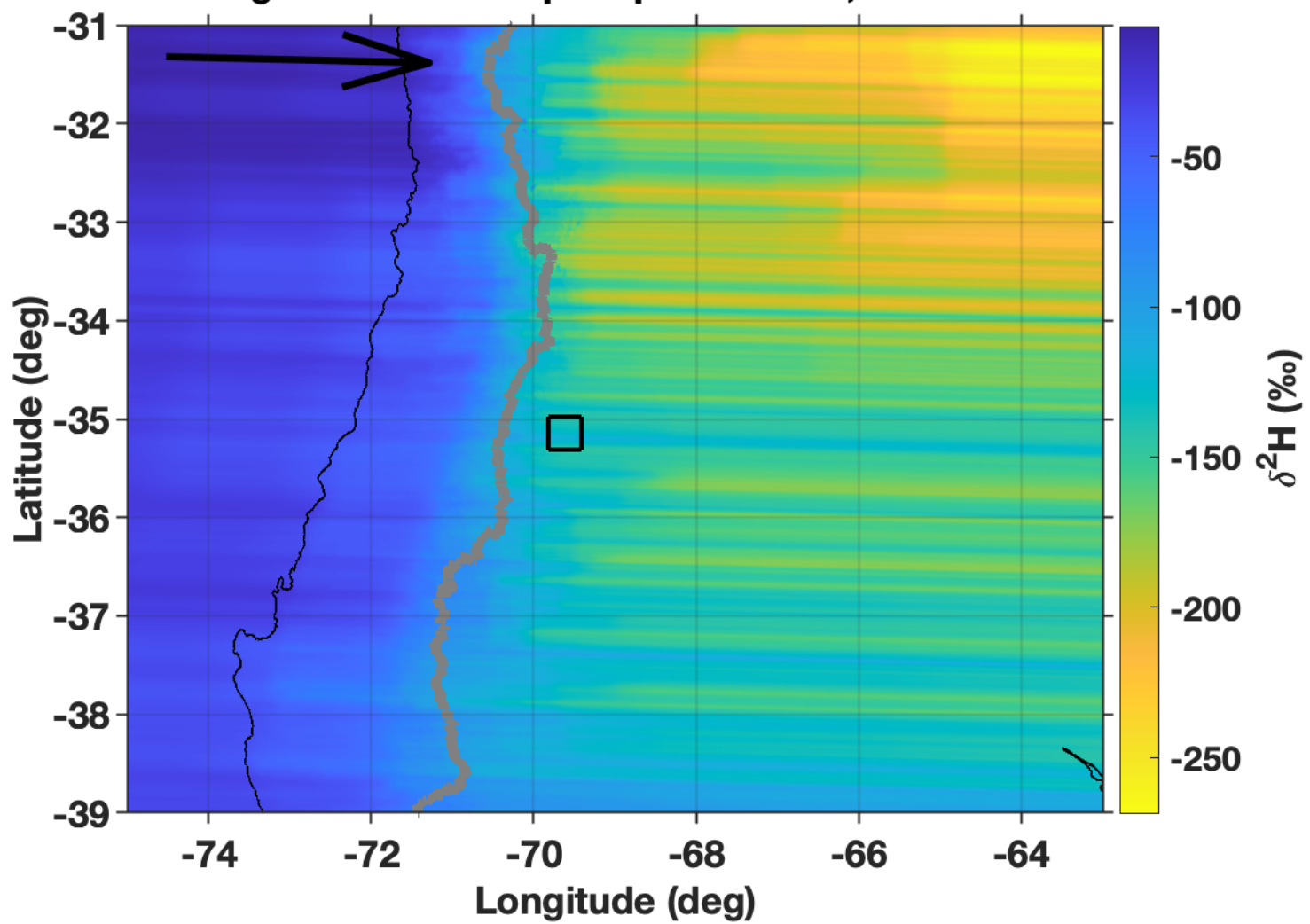


Fig. 15. Predicted precipitation $\delta^2\text{H}$, state #2

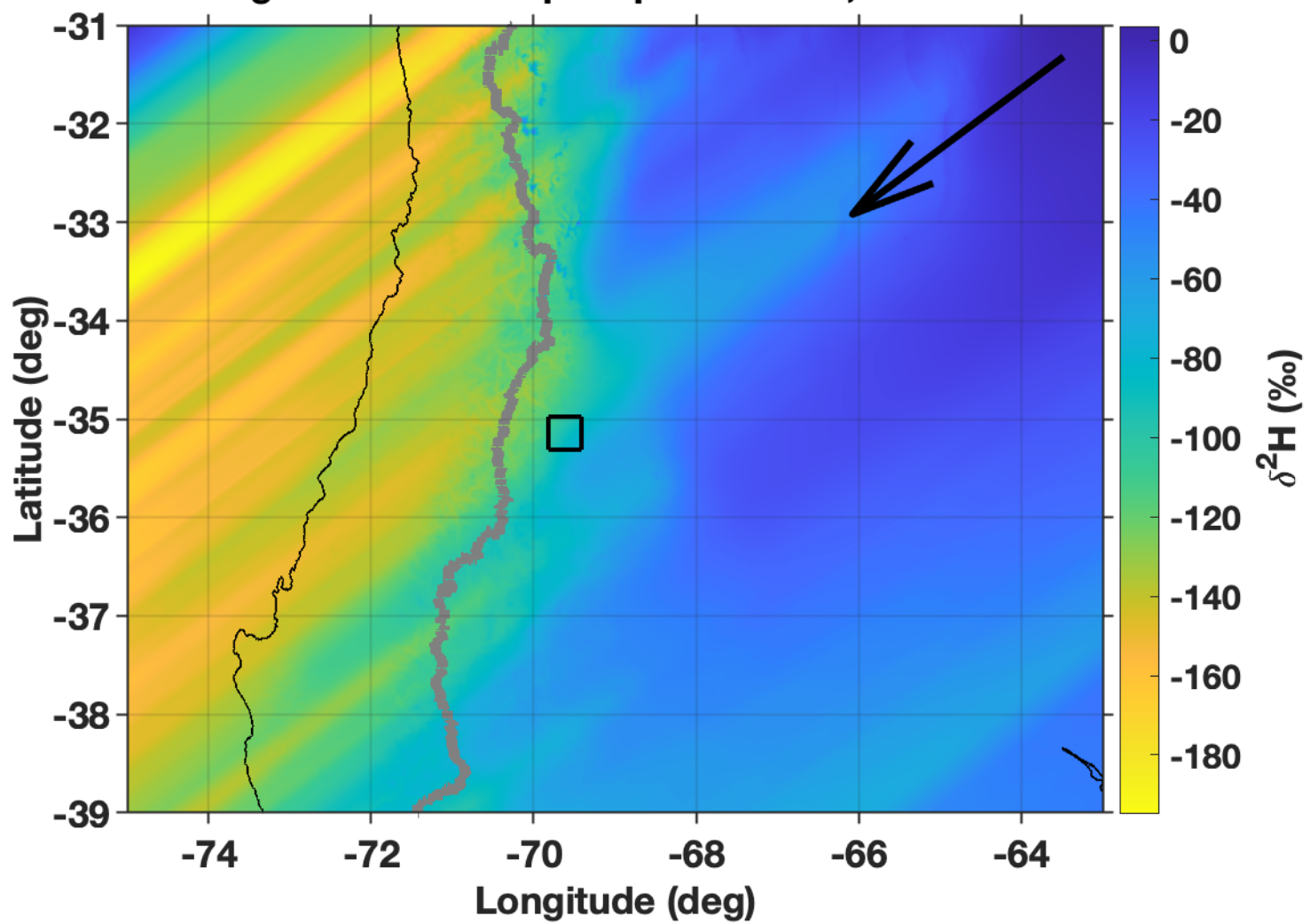


Fig. 16. Surface-air temperature, state #1

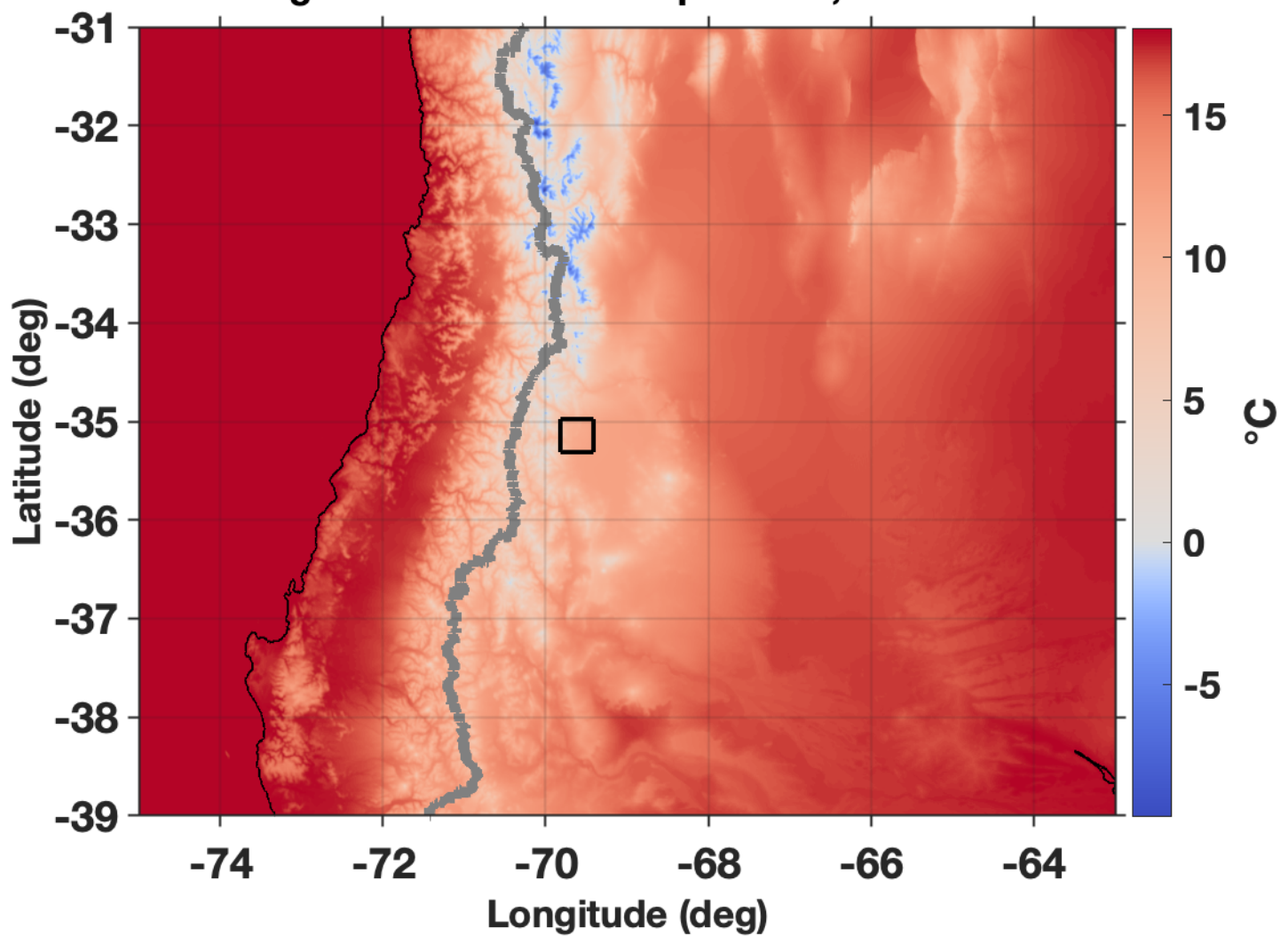


Fig. 17. Surface-air temperature, state #2

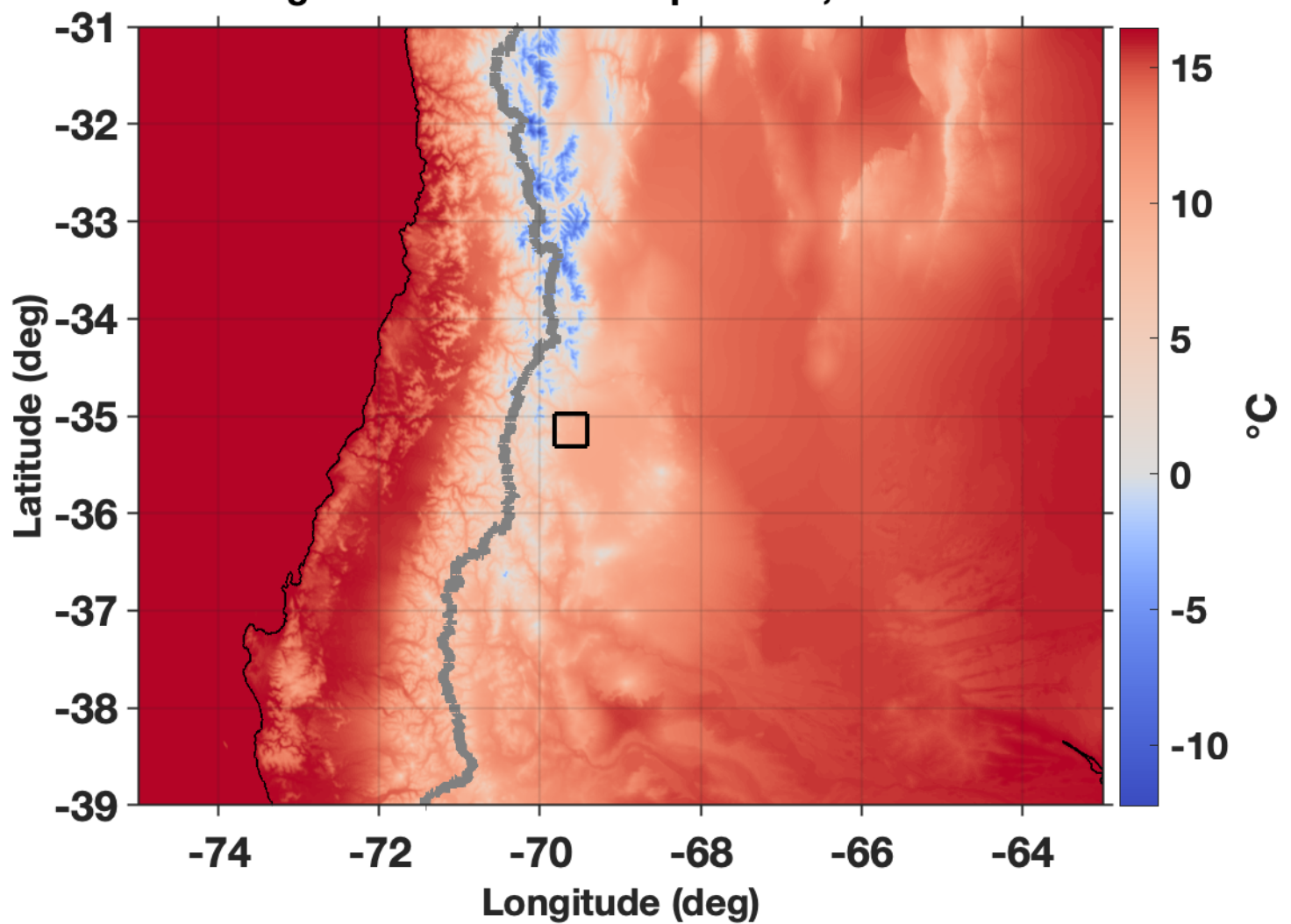


Fig. 18. Surface velocity ratio, state #1

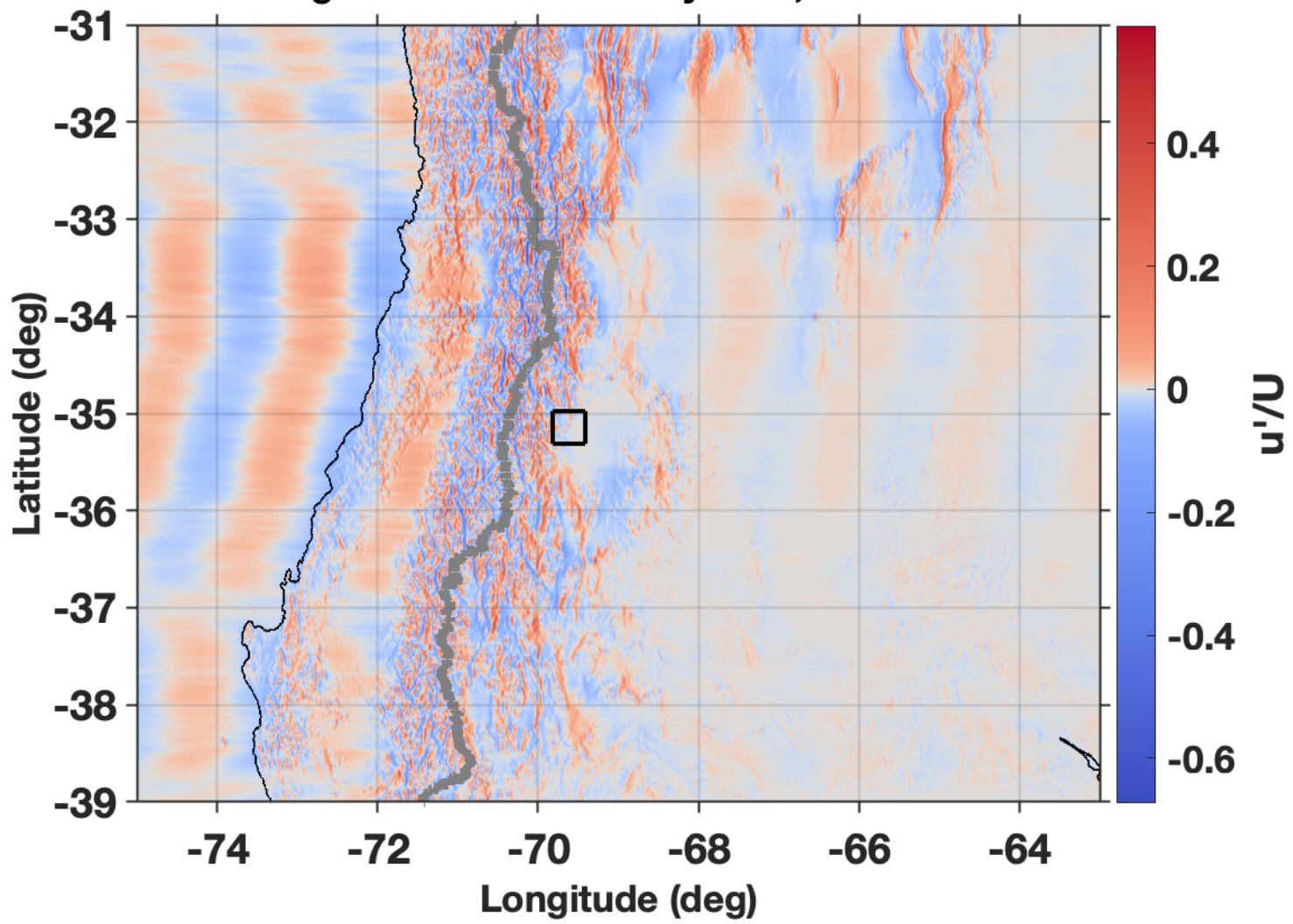


Fig. 19. Surface velocity ratio, state #2

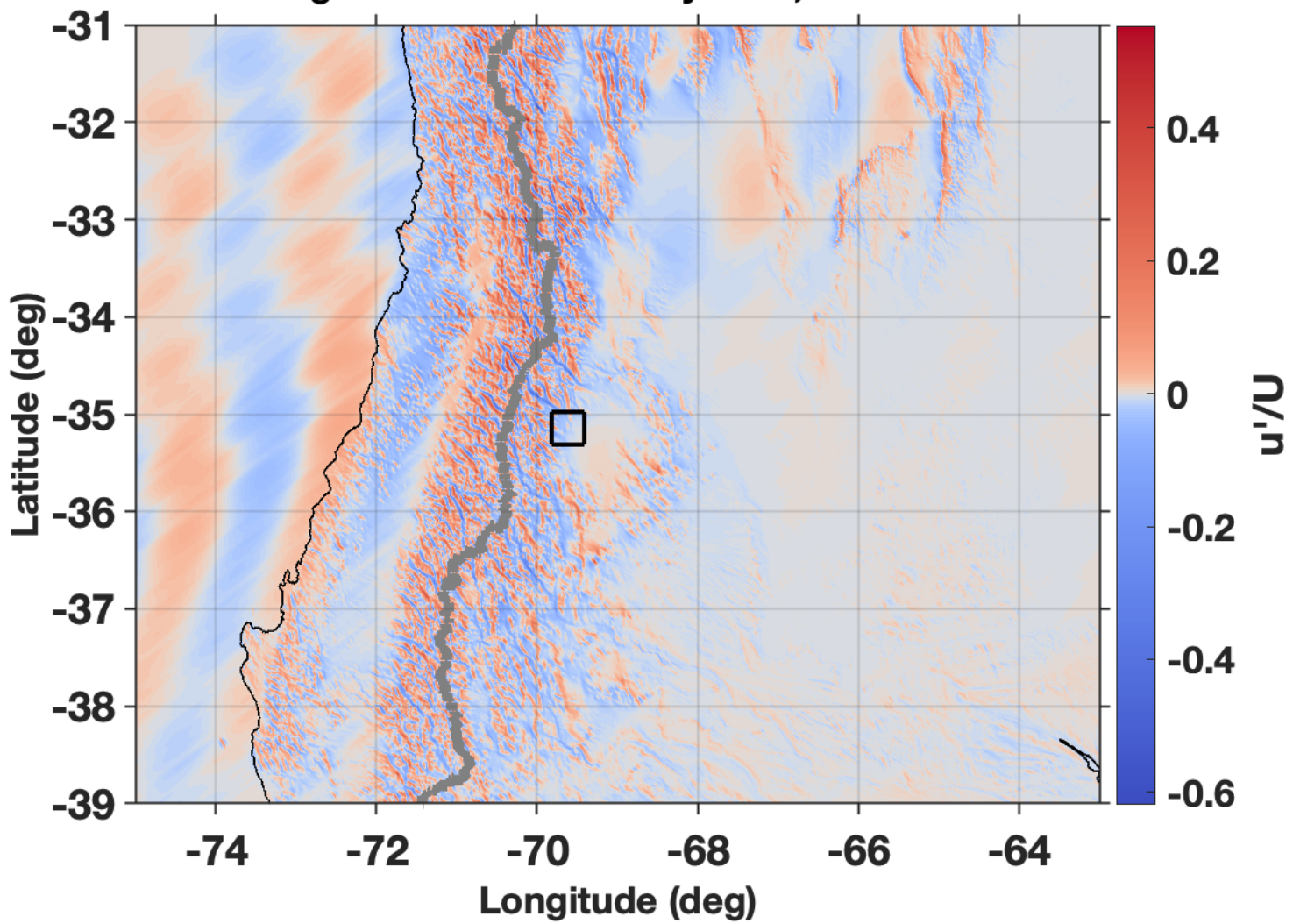
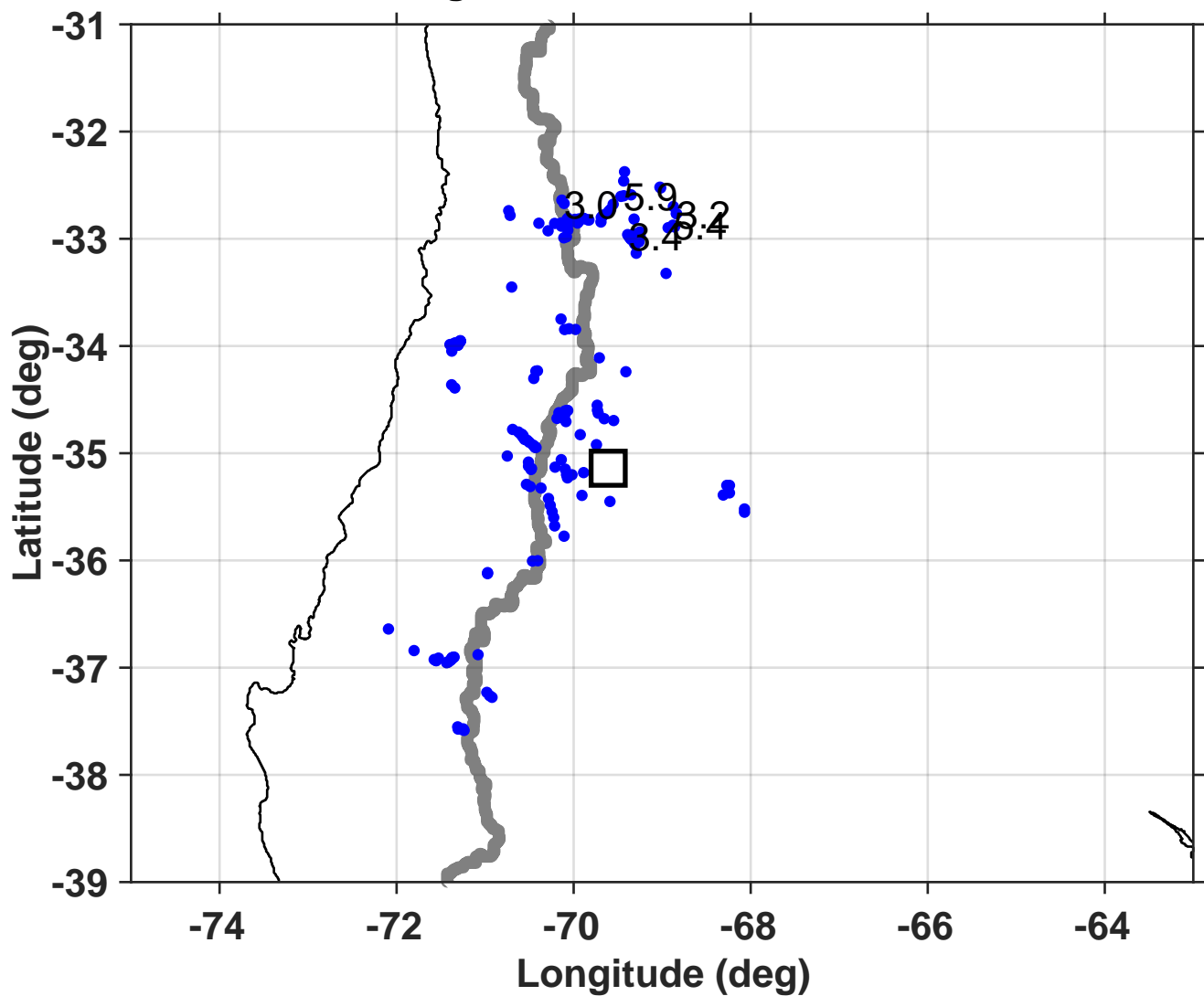


Fig. 20. Location of outliers



Program: opiPredictCalc
Start time: 11-Aug-2022 16:43:52

opiPredictCalc

----- Climate Data -----

Path for climate data:
private/
Mat file for benthic foram climate data:
Miller2020BenthicForamClimate.mat
Mat file for moist energy balance data:
MEBM_vary_OLR.mat
Age range used for loess smoothing: 5 Ma

----- OPI Solution -----

Results matfile path:
/Users/markbrandon/Dropbox/OPI Mendoza/runs/run043_Mendoza, leeside evaporation, fit for kappa BEST SOLUTION
Results matfile name:
opiCalc_TwoWinds_Results.mat
Run file path:
/Users/markbrandon/Dropbox/OPI Mendoza/runs/run043_Mendoza, leeside evaporation, fit for kappa BEST SOLUTION
Run file name:
run043.run
Run title:
run 043, Mendoza area, opi 3.6, two wind, leeside evaporation, fit for kappa
Path name for data directory:
~/Dropbox/OPI Mendoza/data Mendoza

----- Topography File -----

Topography file: Mendoza topography_Gebco1km_-85,-43,-42.5,-27.5.mat
Maximum elevation (m): 6317.73
Grid size, nx and ny: 3827, 1669
Minimum and maximum for longitude: -85, -43
Minimum and maximum for latitude: -42.5, -27.5
Grid spacing, dx and dy (degrees): 0.0109775, 0.00899281
Grid spacing, dx and dy (km): 1007.35, 999.954
Lon, lat for map origin (degrees): -70.2402, -34.3854
Size of cosine window as fraction of grid size: 0.250000
Coriolis frequency at map-origin latitude (mrad/s): -0.0823652

----- Constants -----

Average distance for isotopic exchange (m): 540
Standard-deviation ratio for data residuals: 28.3

----- Best-Fit Solution -----

Selected state for two-wind solution: 2
Wind speed: 3.0204 m/s
Wind azimuth: 233.228 degrees
Sea-level temperature: 289.614 K (16.464 C)
Mountain-height number: 0.265313 (dimensionless)
Horizontal eddy diffusivity: 72557.6 m^2/s
Characteristic time for conversion: 250.814 s
d2H for base precipitation: -7.88753 per mil
d2H latitude gradient for base precipitation: -4.50388 per mil/deg lat
Residual precipitation after evaporation: 0.975209 (fraction)

----- Observed Meteoric Water Line -----

Intercept and slope: 11.0944 per mil, 8.13663

----- List File -----

Read sample list which is an xlsx file with data for specified samples.

The first line gives the temperature derivative for the base-precipitation d2H,
the second line gives the standard error for the modern precipitation d2H,
and the third line gives the standard error for the modern base-precipitation d2H.

Each remaining line provides data for a sample:

name, longitude, latitude, d2H_obs, SE(d2H_obs), age, comment

List file path:

/Users/markbrandon/Dropbox/OPI Mendoza/runs/run043_Mendoza, leeside evaporation, fit for
kappa BEST SOLUTION

List file name:

mendozaList.xlsx

Temperature derivative for present d2H₀ (K/per mil): 2.370000

The value above is estimated using the slope for monthly averages
for precipitation d2H and temperature.

Standard error for modern precipitation d2H (per mil): 0.840000

Standard error for modern base-precipitation d2H (per mil): 0.720000

Number of selected samples: 109

Time for computation: 0.69 hours

Program: opiPredictPlot
Start time: 11-Aug-2022 23:30:12

opiPredictPlot

----- Source files used for opiPredictCalc -----

Path for climate matfiles:

private/

Mat filename for BenthicForamClimate data:

Miller2020BenthicForamClimate.mat

Mat filename for MEBM data:

MEBM_vary_OLR.mat

----- opiPredictCalc matfile used here -----

Path:

/Users/markbrandon/Dropbox/OPI Mendoza/runs/run043_Mendoza, leeside evaporation, fit for kappa BEST SOLUTION/opiPredict results using Miller et al 2020

Filename:

opiPredictCalcMiller_State02.mat

List file path:

/Users/markbrandon/Dropbox/OPI Mendoza/runs/run043_Mendoza, leeside evaporation, fit for kappa BEST SOLUTION

List file name:

mendozaList.xlsx

----- Background Information -----

Option for precipitation data: local

Average age interval between samples (Ma): 0.510303

Average age interval between record values (Ma): 0.00131

Age span for lowess smoothing (Ma): 5

Average standard error for sample d2H (per mil): 3.90081

Standard error for OPI estimate of modern d2H (per mil): 0.84

Standard error for OPI estimate of d2H0 (per mil): 0.72

Standard deviation for high-frequency variation in d2H0 (per mil): 2.23512

Standard deviation for high-frequency variation in d2H (per mil): 3.12876

PhiClimate $\approx 1 + kClim \ln(T0Ref/T0Pres)$, kClim (dimensionless): -12.0001

Average, min, and max for partial standard error for PhiLift: 0.0669798, 0.0154643 to 0.128692

Average, min, and max for total standard error for PhiLift: 0.185477, 0.105428 to 0.285831

opiPredict_Plot, Figure Captions

Figure 1. Hydrogen isotopic composition of precipitation as a function of age. Top plot: Measured precipitation $\delta^2\text{H}$ values are shown with red points and error bars (analytical uncertainty, +/- 1 standard error). The associated black line shows the long-term variation of these measurements (smoothed using LOWESS regression with a 5 Ma span). The blue points in the lower part of the plot show predicted $\delta^2\text{H}$ precipitation values for each of the samples after accounting for climate at the sample age but otherwise maintaining the topography the same as modern. The associated blue line shows the long-term variation of this predicted reference case (LOWESS regression, 5 Ma span). The gray line at the top of the plot shows the predicted isotopic composition for base precipitation at the latitude of the samples, and account for the difference in climate relative to modern. The associated blue line shows the long-term variation (LOWESS regression, 5 Ma span). Bottom plot: Predicted sea-surface air temperature at the latitude of the samples and as a function of age.

Figure 2. Predicted evolution of Φ_{lift} , which is the ratio of the observed isotopic fractionation estimated for the sample location and age, relative to predicted isotopic fractionation at same location and age but for a topography that remains the same as modern. These fractionations have been corrected for the change in climate with age. The red points show Φ_{lift} for the samples, and the error bars show ± 1 standard error uncertainties. The uncertainties include analytical errors, and errors associated with estimating the influence of temperature on the isotopic composition of base precipitation, and the isotopic fractionation caused by orographic lifting. The black line shows the long-term variation of Φ_{lift} (LOWESS regression, 5 Ma span), and the black dashed line marks $\Phi_{\text{lift}} = 1$, which is the prediction for a topography that remains the same as modern.

Fig. 1. Observed and Predicted Isotopic Fractionation

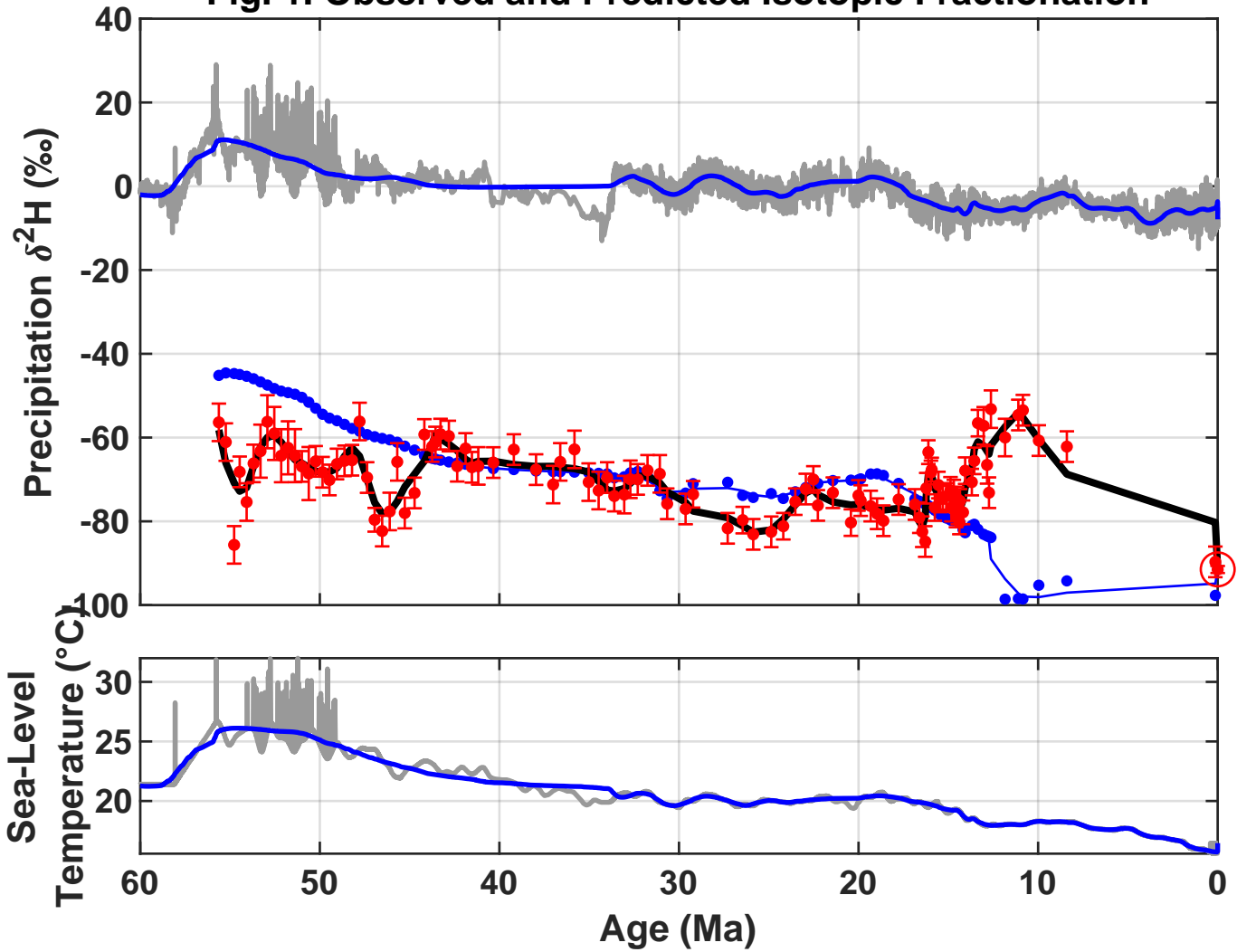


Fig. 2. Predicted Evolution of Φ_{lift}

